energies

MDPI

Article

Optimal Operation of an Integrated Hybrid Renewable Energy System with Demand-Side Management in a Rural Context

Polamarasetty P Kumar [1,*], Ramakrishna S. S. Nuvvula [1], Md. Alamgir Hossain [2], SK. A. Shezan [3], Vishnu Suresh [4,*], Michal Jasinski [4,*], Radomir Gono [5] and Zbigniew Leonowicz [4]

1 Department of Electrical and Electronics Engineering, GMR Institute of Technology, Rajam 532127, India; nramkrishna231@gmail.com
2 Queensland Micro and Nano-Technology Centre, Griffith University, Nathan, QLD 4113, Australia; mdalamgir.hossain@griffith.edu.au
3 Department of Electrical Engineering, Engineering Institute of Technology, Melbourne, VIC 3001, Australia; shezan.ict@gmail.com
4 Faculty of Electrical Engineering, Wroclaw University of Science and Technology, 50-370 Wroclaw, Poland; zbigniew.leonowicz@pwr.edu.pl
5 Department of Electrical Power Engineering, Faculty of Electrical Engineering and Computer Science, VSB—Technical University of Ostrava, 708 00 Ostrava, Czech Republic; radomir.gono@vsb.cz
* Correspondence: praveenkumar.p@gmrit.edu.in (P.P.K.); vishnu.suresh@pwr.edu.pl (V.S.); michal.jasinski@pwr.edu.pl (M.J.)

Abstract: A significant portion of the Indian population lives in villages, some of which are located in grid-disconnected remote areas. The supply of electricity to these villages is not feasible or cost-effective, but an autonomous integrated hybrid renewable energy system (IHRES) could be a viable alternative. Hence, this study proposed using available renewable energy resources in the study area to provide electricity and freshwater access for five un-electrified grid-disconnected villages in the Odisha state of India. This study concentrated on three different kinds of battery technologies such as lithium-ion (Li-Ion), nickel-iron (Ni-Fe), and lead-acid (LA) along with a diesel generator to maintain an uninterrupted power supply. Six different configurations with two dispatch strategies such as load following (LF) and cycle charging (CC) were modelled using nine metaheuristic algorithms to achieve an optimally configured IHRES in the MATLAB© environment. Initially, these six configurations with LF and CC strategies were evaluated with the load demands of a low-efficiency appliance usage-based scenario, i.e., without demand-side management (DSM). Later, the optimal configuration obtained from the low-efficiency appliance usage-based scenario was further evaluated with LF and CC strategies using the load demands of medium and high-efficiency appliance usage-based scenarios, i.e., with DSM. The results showed that the Ni-Fe battery-based IHRES with LF strategy using the high-efficiency appliance usage-based scenario had a lower life cycle cost of USD 522,945 as compared to other battery-based IHRESs with LF and CC strategies, as well as other efficiency-based scenarios. As compared to the other algorithms used in the study, the suggested Salp Swarm Algorithm demonstrated its fast convergence and robustness effectiveness in determining the global best optimum values. Finally, the sensitivity analysis was performed for the proposed configuration using variable input parameters such as biomass collection rate, interest rate, and diesel prices. The interest rate fluctuations were found to have a substantial impact on the system's performance.

Keywords: off-grid; integrated renewable energy; demand-side management; optimization techniques; different batteries

Citation: Kumar, P.P.; Nuvvula, R.S.S.; Hossain, M.A.; Shezan, S.A.; Suresh, V.; Jasinski, M.; Gono, R.; Leonowicz, Z. Optimal Operation of an Integrated Hybrid Renewable Energy System with Demand-Side Management in a Rural Context. *Energies* **2022**, *15*, 5176. https://doi.org/10.3390/en15145176

Academic Editor: Albana Ilo

Received: 7 May 2022
Accepted: 7 July 2022
Published: 17 July 2022

1. Introduction

1.1. Need for Energy Management Systems

Energy and freshwater are essential to humankind, but the planet is suffering greatly from future and current energy demands as well as freshwater requirements due to the

rapid climate change and population growth [1]. To resolve this power shortage, a backup power system is needed. Diesel generators (DGs) have been employed as a backup mechanism for a range of off-grid applications, but they face a number of key issues, including fuel price volatility and high operating and maintenance costs. However, the optimum combination of RE resources and DGs results in a cost-effective, efficient, and clean energy system that reduces the uncertainties, energy prices, and CO_2 emissions. At the same time, an off-grid RE-based power system comprised of one or two RE resources in conjunction with the battery storage system and DG is an ideal combination for electrifying the off-grid rural areas. In the context of microgrid sizing, microgrids are typically either undersized or oversized to meet the energy demands. An undersized microgrid would result in a loss of power supply while an oversized microgrid would result in high system costs and excess electricity production. Hence, to resolve these issues and reap the benefits of the RE-based microgrid, a strong energy management strategy (EMS) is required [2].

1.2. The Importance of a Reverse Osmosis Desalination Plant for Remote Villagers

In India, safe drinking water is exceedingly limited, particularly in remote rural villages. Although some villages continue to receive government water supply, almost 73% of Indian villages still rely on groundwater supply. Unfortunately, none of these resources are unsuitable for providing a safe drinking water supply. The usage of fertilizers in such areas, as well as other activities such as mining, has polluted the groundwater supply. Streams surrounding human areas, such as villages, are also heavily polluted. Numerous Indian soils have brackish groundwater with total dissolved solid (TDS) concentrations of more than 500 mg/L. It is greater than the Bureau of Indian Drinking Water Standards' recommendation. Children of all ages are affected by this contaminated drinking water. Children under the age of five are especially vulnerable since it frequently kills them and creates serious health-related problems. As a result, the usage of reverse osmosis Desalination (ROD) plants is essential for the health and well-being of rural village dwellers. Membranes and chemicals are now widely available in the market as replacement components of the ROD units, and nowadays, ROD units can be powered by locally available RE resources such as solar, wind, and biomass. As a result, deploying ROD units in isolated rural communities has become both simple and cost-effective, as well as necessary.

1.3. Overview of the Optimization Techniques

Several studies on microgrid size issues have been reported in the literature. The preceding approaches can be divided into three categories: (i) software tools such as RETScreen, HOMER, IHOGA, HOGA [3], etc., (ii) deterministic approaches such as graphical construction, probabilistic, iterative, linear programming, and analytical and numerical methods [4], and (iii) metaheuristic algorithms such as grasshopper optimization algorithm (GOA) [5], grey wolf optimization (GWO) [6], particle swarm optimization (PSO) [7], genetic algorithm (GA) [8], etc. Although the software tools are simple to use, users cannot select the necessary components in it and have no access or control over the algorithms and calculations contained within them. Using software tools, several assumptions and sequences can limit the microgrid size issues. Additionally, the deterministic approaches outperform the software tools [9]. However, because of the complexities of microgrid sizing, at the local optima, the optimal solution is extremely entrapped. In these circumstances, they are unable to converge to the global best optimum solution. As a result, the algorithm must be repeated numerous times with the initial condition chosen at random to avoid this local optima entanglement. Hence, the solution is unlikely to be the global best optimal solution, and the algorithm has to try several times to discover it. Therefore, metaheuristic algorithms have become one of the most promising and extensively used methods [4].

Since the last decade, a number of metaheuristic algorithms have been developed and paved the way for concerns such as microgrid sizing. Interestingly, few of these methods, such as particle swarm optimization (PSO) and genetic algorithm (GA), are well-known not only among the computer scientists but also among a large number of scientists from

other fields. They are adaptive approaches that outperform deterministic methods because their solutions are not substantially entangled at local optima. All of these algorithms have various benefits, including the ability to handle any type of optimization problem [9]. In contrast, the no-free-lunch theorem states that a particular metaheuristic algorithm can achieve the global best optimal solution for a specific objective function but it may produce ineffective outcomes for other objective functions [10]. This has prompted microgrid size researchers to look at the maiden metaheuristic algorithms [4].

1.4. Literature Review on Optimization Techniques and Different Battery Technologies

Rechargeable batteries, soil physics, and chemical engineering are just a few of the many fields that make use of electrolyte diffusion in electrolyte solutions [11,12]. For the standalone un-electrified villages in the Chikmagalur district of Karnataka, Ramesh and Saini [13] used the HOMER Pro to conduct a feasibility analysis for the PV/diesel generator (DG)/micro hydro power (MHP)/WT/BAT configuration with LA and Li-Ion battery technologies and three dispatch strategies such as cycle charging (CC), combined dispatch (CD), and load following (LF) and it was revealed that the Li-Ion battery-based IHRES with CD strategy had the lowest net present cost (NPC) and cost of energies (COEs) when compared to CC and LF strategies.

Alpesh and Sunil [14] used a PV/biogas generator (BGG)/biomass generator (BMG)/WT/LA battery configuration to power a simple off-grid village of 123 hamlets near the Gujarat-Rajasthan state border in India and conducted an assessment using the technique of optimum component selection with widely available types of equipment using a multi-variable linear regression algorithm (MVLRA) and PSO to obtain the optimal results with the MVLRA.

Rajanna and Saini [15] employed a genetic algorithm to electrify five independent un-electrified hamlets in India's Chamarajanagar district of Karnataka state using a configuration of PV/BMG/BGG/WT/MHP/LA battery technology. Ankit et al. [16] used the HOMER Pro® software tool to electrify five independent un-electrified hamlets in the Almora district of Uttarakhand state in India using a PV/BGG/DG/MHP/BMG/LA battery configuration to minimize the system's NPC.

Upadhyay and Sharma [17] used CC and LF strategies with GA, biogeography-based optimization (BBO), and PSO algorithms to power seven standalone villages in the Indian state of Uttarakhand with a configuration of PV/BMG/DG/BGG/MHP/LA battery technology. From the results, it was observed that the BBO algorithm produced the optimal results. Chong Li et al. [18] used the HOMER pro® software tool to conduct a study for 280 single-family homes in Gansu Province, China, employing a WT/DG/BAT configuration with Li-Ion, LA, and zinc-bromine (ZB) battery technologies. According to the findings, the ZB battery technology produced the optimal results.

Bart et al. [19] used a Simapro software tool to conduct a life cycle assessment of PV lighting products in a solitary rural area in South-East Asia and found that solar PV lighting has a lower environmental effect than traditional lighting options. Shezan et al. [20] used the HOMER Pro® software tool to conduct a study in a solitary rural region of KLIA Sepang Station in the Malaysian state of Selangor, employing a configuration of PV/DG/WT/LA battery technology to lower the system's NPC. Carlos et al. [21] used GA-based algorithms to analyze how to power an Indonesian island with PV/DG/Li-Ion battery technologies.

Chhunheng and Supachart [22] used the HOMER Pro® software tool to analyze how to electrify a solitary rural region in Cambodia utilizing PV/DG/LA battery technology to lower the system's NPC. Sompol et al. [23] used the LABVIEW software tool to conduct a study for off-grid applications in Thailand with a BMG/PV/Li-Ion battery configuration. Haein and Tae [24] used the HOMER Pro® software tool to conduct an analysis to power a freestanding region in Myanmar utilizing a PV/DG/BAT configuration with LA and Li-Ion battery technologies to lower the system's NPC, and from the results, it was identified that the LA battery technology provided the optimal results.

Lorafe et al. [25] used the HOMER Pro® software tool to analyze how PV/LA battery technology could be used to power South-East Asian islands: Philippines, Gilutongan,

Cebu, and Cordova with minimum NPC. Sarah et al. [26] conducted an analysis in Dodoma and Tanzania utilizing the PV/DG/WT/BAT configuration with LA and Li-Ion battery technologies and found that the Li-Ion battery-based configuration with GA had the lowest COE.

Kaabeche and Bakelli [27] conducted an assessment using a WT/PV/BAT configuration with Li-Ion, LA, and nickel-cadmium battery technologies. The ALO, GWO, JAYA, and Krill Herd algorithms were used to examine the system's unit electricity cost and it was discovered that the JAYA algorithm provided a viable solution with an LA battery-based system, followed by Li-Ion and Ni-cd batteries.

1.5. Demand-Side Management

In general, uncoordinated peak and valley load demands increase energy costs by expanding the generation and distribution networks, as well as forcing generators to run out of their rated capacity during peak load periods [11]. Hence, it would be advantageous to lower some of these demands in order to avoid the need for costly extra installations [12]. Furthermore, the energy demand curves must be as smooth as possible for several reasons, including minimizing the strain on power generation equipment and other protective components of the microgrid, as well as lowering energy costs and deferring or avoiding future equipment investment. In this context, several demand-side management (DSM) strategies in the power system industry have been applied using a variety of methods such as "peak clipping, valley filling, load shifting, energy conservation, load building and flexible load shape" [13], which are illustrated in Figure 1 and described as follows [28]:

(a) Peak clipping: peak clipping is a technique for reducing load demand during peak hours. It is frequently accomplished by either limiting the use of appliances during peak hours or motivating customers to modify their demand behavior by offering attractive price signals.

(b) Valley filling: the purpose of valley filling is to stimulate energy use during off-peak hours in order to increase average energy utilization. It can be done by encouraging customers to do things such as loading and charging during off-peak hours when utilities prefer to use less energy to meet the load demand.

(c) Load shifting: this is intended to shift the loads from on-peak to off-peak hours without altering the energy use pattern. For example, during off-peak hours, customers can store thermal heat and use it to keep the room warm all day. Similarly, other household activities such as washing clothes and washing dishes can be done at night to prevent peak loading.

(d) Energy conservation: the goal of energy conservation is to reduce the energy demand by using energy-efficient devices. Changing to efficient devices can reduce the load demand as well as change the load shape.

(e) Load building: load building and flexible loads are connected to the network supported under the principle of smart grids. Load building improves load sharing as well as energy storage systems to improve grid responsiveness.

(f) Flexible load shape: flexible loads can be handled in return for the benefits. This implies that the load shape is responsible for the reliability conditions which means that the loads can be modified according to the reliability of the system.

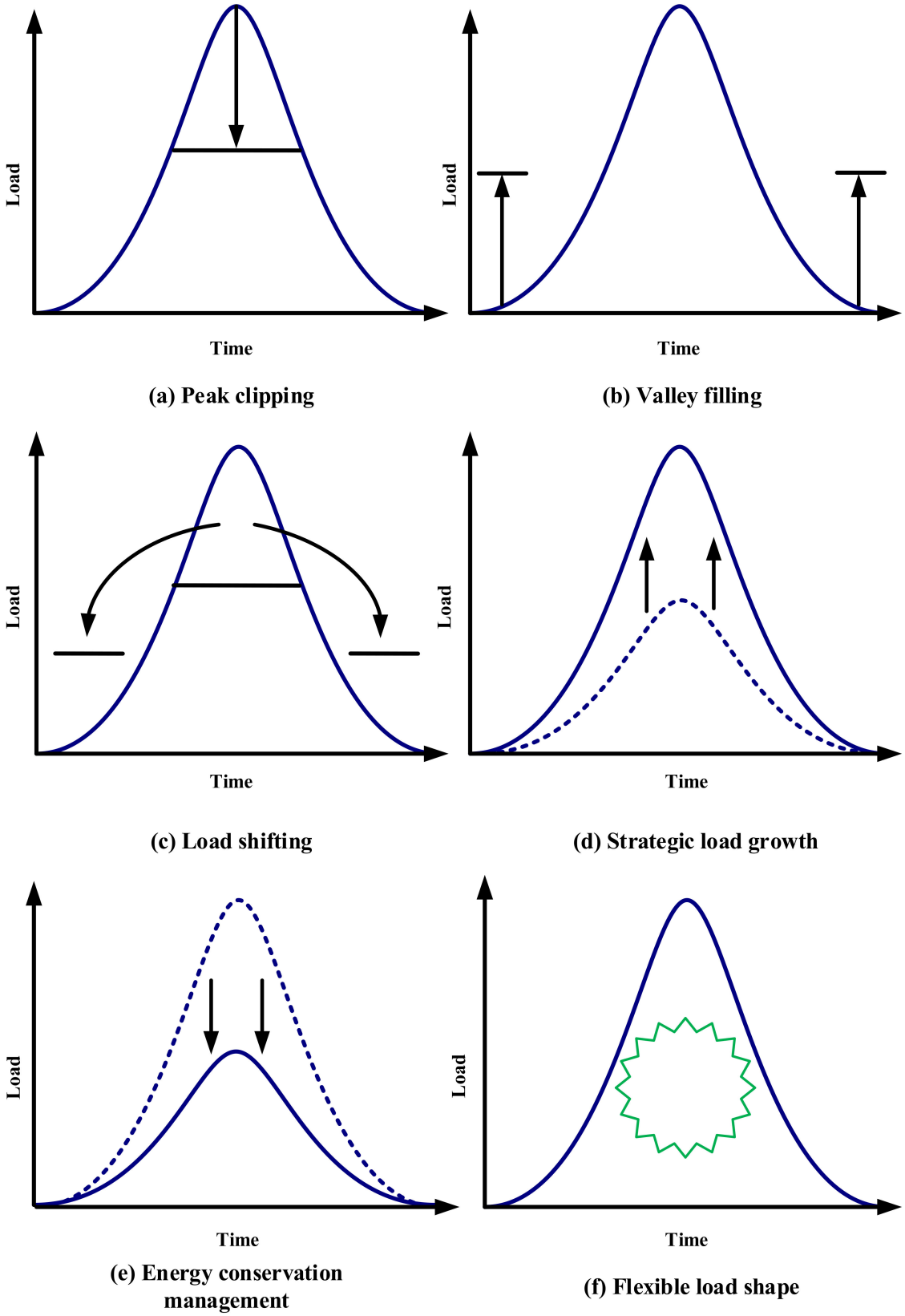

Figure 1. All types of demand-side management.

1.6. Literature Review of Demand-Side Management

The concept of DSM has inspired the attention of researchers working on autonomous IHRESs. Rajanna and Saini [29] used GA and PSO algorithms to analyze the performance of

four un-electrified village zones in India with a DSM strategy using three investment-based scenarios, such as low investment with high rating appliances, medium investment with moderate rating appliances, and high investment with low rating appliances and found that the systems with DSM strategy had the lowest costs using PSO.

Upadhyay and Sharma [17] proposed three energy management schemes based on the HOMER pro® software tool and GA and PSO algorithms, claiming that peak shaving with the CC strategy utilizing the PSO method would be more cost-effective than other methods. Chauhan and Saini [30] investigated the techno-economic aspects of an IHRES using an energy management approach by considering a load-shifting strategy based on DSM to meet the energy demands of the population of Uttarakhand state villages in India, finding that the DSM strategy was a more cost-effective solution than the NON-DSM strategy.

Zheng et al. [31] used linear economic programming to design a tariff-based load-shifting algorithm to lower the operational costs of a biomass-based microgrid with combined heat and power. Wang et al. [32] combined the receding horizon optimization technique with DSM to lower the maximum operating and environmental expenses of a standalone PV/WT network-based single-family dwelling. To obtain the best performance in standalone systems, Marzband et al. [33] presented a stochastic optimization technique that takes into account fluctuations in the design of load utilization.

Matallanas et al. [34] suggested a DSM control technique for enhancing business planning in PV systems using neural networks with the goal of increasing energy efficiency. Gudi et al. [35] used a binary particle swarm optimization to apply the DSM strategy in the home sector for cost savings of the suggested system. Kyriakarakos et al. [36] proposed a smart DSM solution based on the grey prediction algorithm to meet system architectural principles and ensure the effectiveness of a freestanding multi-generated microgrid operating in remote places. Randa Kallel et al. [37] investigated the benefits of the proposed integrated system strategic plan under various scenarios and conducted a comparison between the DSM and NON-DSM energy management strategies.

1.7. Motivation for the Article to Consider Energy Conservation-Based DSM

An energy conservation-based electrification is highly recommended in India. On 5 January 2015, the Government of India launched Unnat Jeevan by Affordable LEDs and Appliances for All (UJALA) scheme, which will provide people with cost-effective energy-efficient LED bulbs compared to market prices through Energy Efficiency Services Ltd. (EESL) in a joint venture managed by the Indian Ministry of Power providing widespread distribution of LED bulbs and energy-efficient electrical appliances. It has been distributed more than 21.7 crores of energy-efficient LED bulbs with its network spread over 24 states in India, resulting in energy and electrical bill savings as well as the reduction in both the CO_2 emissions and peak load demands. The National Energy Efficient Fan Program (NEEFP) was also introduced by the EESL to promote energy conservation through increased residential use of energy-efficient fans and EESL also developed a service model such as the Street Lighting National Program (SLNP) scheme that allows municipalities to replace conventional lights with LEDs without any upfront costs, where the balance of costs is recovered by monetizing the energy savings through local municipalities [38]. These are all schemes of the Government of India that inspired us to write this article about energy conservation-based DSM.

1.8. Novelty and Overview of the Article

It was identified that there has been no research on the supply of freshwater to the isolated regions in the Indian scenario using a configuration of PV/BMG/DG/BAT with Ni-Fe, LA, and Li-Ion battery technologies using LF and CC strategies. Furthermore, several researchers conducted a techno-economic feasibility study to provide an uninterruptable power supply using only one or two types of battery technologies, such as Li-Ion and LA. Moreover, various researchers have conducted studies on different types of DSM approaches. However, no studies have been attempted to consider the efficiency-based

scenarios (energy conservation-based DSM) such as high power rated appliances of low cost (HPRALC), medium power rated appliances of moderate cost (MPRAMC), and low power rated appliances of high cost (LPRAHC) with different dispatch strategies using different battery technologies for off-grid rural areas, which was identified as a significant gap in the existing literature. Finally, several researchers have compared the proposed algorithm's convergence and robustness efficiency to those of only one or two other algorithms.

For a realistic analysis of an off-grid IHRES, the aforementioned gaps and limitations must be resolved. To keep in this view, five un-electrified off-grid villages in the Odisha state of Rayagada district were identified as a study area in order to provide power and freshwater availability using accessible RE resources in the study area, such as biomass and solar. Owing to the intermittent nature of these RE resources, the power supply is not continuous. To ensure a continuous power supply, the study conducted feasibility studies with three different types of battery technologies such as lithium-ion (Li-Ion), nickel-iron (Ni-Fe), and lead-acid (LA), as well as a diesel generator (DG), by taking into account LF and CC strategies. In general, the rural people's load usage pattern is almost the same throughout the day. Regularly, the peak loads occur in the evening due to the priority loads such as lamps, fans, and TVs; these loads cannot be altered by their habitual pattern of use. Therefore, peak clipping and load shifting are not possible for off-grid rural villagers, especially in the evening time. However, with proper energy conservation management, these peak loads can be reduced without peak clipping and load shifting. It is one of the most successful and favored demand response programs for off-grid rural villagers due to its easy-to-adopt benefits, no maintenance, and no need of shifting priority loads. Hence, the study considered energy conservation-based DSM using consumers' loads usage patterns such as high power rated appliances of low cost (HPRALC), medium power rated appliances of moderate cost (MPRAMC), and low power rated appliances of high cost (LPRAHC) with different dispatch strategies using different battery technologies.

Six different configurations were modelled in order to determine the optimum configuration for electrifying the study area using available RE resources and the proposed battery technologies with their different depth of discharges (DODs) such as PV/BMG/DG/LA at 70% DOD, PV/BMG/DG/LA at 80% DOD, PV/BMG/DG/Li-Ion at 50% DOD, PV/BMG/DG/Li-Ion at 70% DOD, PV/BMG/DG/Li-Ion at 80% DOD, and PV/BMG/DG/Ni-Fe at 80% DOD, which were tested with two different dispatch strategies such as LF and CC using consumers load usage patterns such as HPRALC, MPRAMC, and LPRAHC-based scenarios. To obtain an optimum configuration from these six configurations, a maiden algorithm called a Salp Swarm Algorithm from the metaheuristic family was proposed in the study [10]. To demonstrate its convergence and robustness efficiency in identifying the global best optimal values, it was compared with eight other proven and well-known algorithms, namely: particle swarm optimization (PSO) [7], differential evolutionary algorithm (DE) [39], genetic algorithm (GA) [8], ant lion optimization (ALO) [40], grasshopper optimization algorithm (GOA) [5], grey wolf optimization (GWO) [6], moth flame optimization (MFO) [41], and dragonfly algorithm (DA) [42]. Finally, the optimal configuration's sensitivity analysis was investigated using various input parameters such as biomass foliage collection rate, interest rate, and diesel prices.

2. Development of the IRES

A systematic process is essential for the implementation of an IHRES for isolated rural communities, which is outlined in the following steps:

2.1. Step 1—Study Area Identification

In the Rayagada district of Odisha state in India, a group of five un-electrified villages of Muniguda block were considered as a study area. Figure 2 shows its geographic location on the map. It is located at 19°37′16.6944″ N latitude and 83°29′50.6688″ E longitude, at a height of 206 m from the above mean sea level. In this area, a total of 1213 people live in 266 households, none of which have access to electricity or a safe drinking water supply.

Because of its remote location, it has yet to be electrified, so people still rely on solar lamps, kerosene lanterns, and candles for lighting.

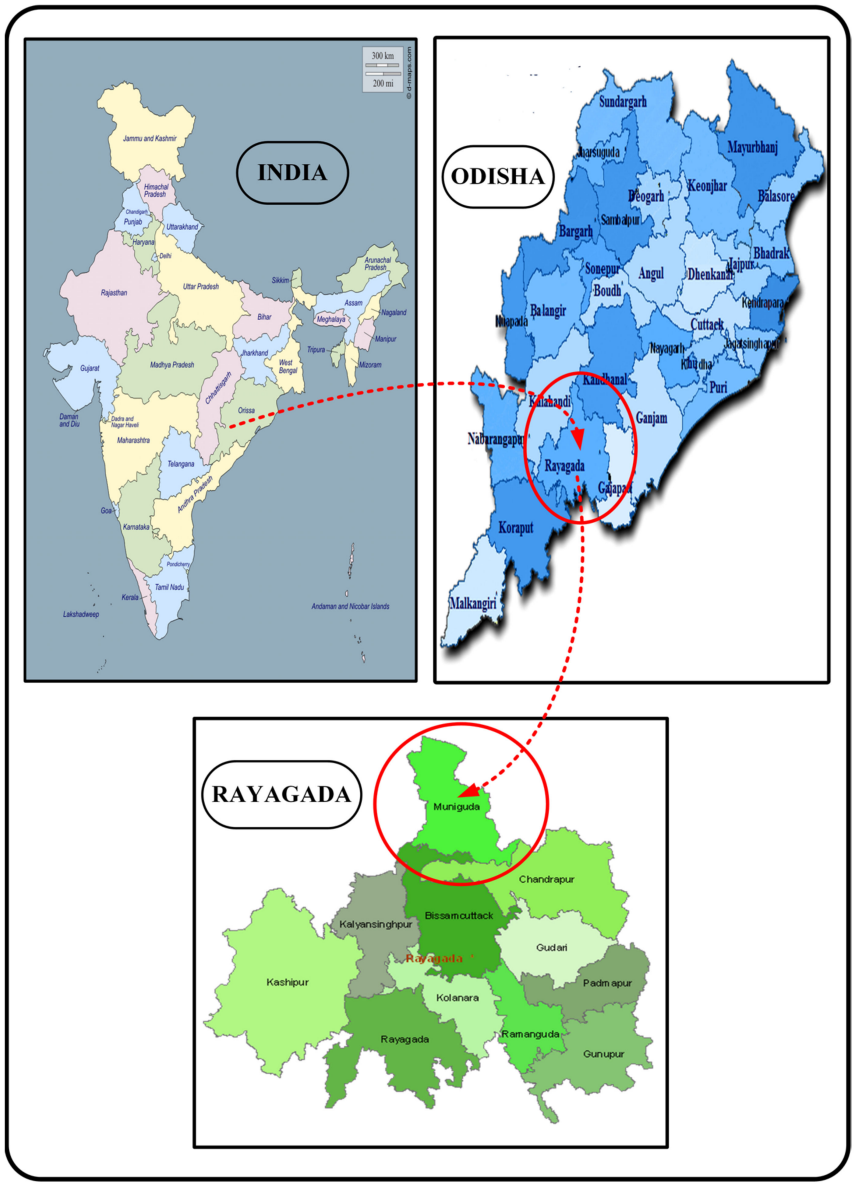

Figure 2. The location of the study area on the map.

2.2. Step 2—Estimation of Electrical Energy Demand and Hourly Freshwater Requirements

This study contains three different types of energy-efficiency scenarios based on the household electrical appliance usage patterns such as high power rated appliances of low cost (HPRALC), medium power rated appliances of moderate cost (MPRAMC), and low power rated appliances of high cost (LPRAHC). Each scenario was classified into community, domestic, commercial, agricultural, or small-scale industrial sectors. HPRALC appliances are incandescent bulbs, LCD TVs, incandescent street light lamps, and low-efficiency ceiling fans. MPRAMC appliances are CFL lights, LCD TVs, CFL street lights, and medium-efficiency ceiling fans. LPRAHC appliances are LED TVs, LED lights, LED street lights, and high-efficiency ceiling fans. The corresponding hourly load demands for both the summer and winter seasons and their related details are given in Tables 1–3 and the associated load curves are shown in Figure 3.

Table 1. HPRALC-based scenario load demand for both winter and summer seasons.

Load Sector →	**Domestic Load**				**Community Load**									**Agricultural Load**		**Commercial Load**				**SIL**	
	School				**Hospital**						**Community Hall**		**SL**	**PW**	**MCTM**	**Shops**		**MDP**	**Flour Mill**	**Saw Mills**	
Appliance →	**LED Lamp**	**Fan**	**TV + Dish**	**MC**	**LED Lamp**	**Fan**	**Computer**	**LED Lamp**	**Fan**	**Refrigerator**	**LED Lamp**	**Fan**	**LED Lights**	**Motor (2 hp)**	**Motor (5 hp)**	**LED Lamp**	**Fan**	**Motor (4 hp)**	**Motor (5 hp)**	**Saw Machine**	**Hourly Energy Demand (kWh)**
Rated Power →	**20 W**	**75 W**	**150 W**	**5 W**	**20 W**	**75 W**	**250 W**	**20 W**	**75 W**	**200 W**	**20 W**	**75 W**	**40 W**	**1.5 KW**	**3.73 kW**	**20 W**	**75 W**	**2.983kW**	**3.73kW**	**1.8kW**	
Quantity →	**2**	**1**	**1**	**1**	**12**	**12**	**12**	**5**	**5**	**1**	**3**	**3**	**27**	**6**	**1**	**5**	**5**	**3**	**1**	**1**	
Time (h) ↓		S/W				S/W			S/W			S/W					S/W				S/W
0:00–1:00		19.95/0						0.3	0.38/0	0.2			1.08					2.98			24.89/4.56
1:00–2:00		19.95/0						0.3	0.38/0	0.2			1.08					2.98			24.89/4.56
2:00–3:00		19.95/0						0.3	0.38/0	0.2			1.08					2.98			24.89/4.56
3:00–4:00		19.95/0						0.3	0.38/0	0.2			1.08					2.98			24.89/4.56
4:00–5:00	31.92	19.95/0						0.3	0.38/0	0.2			1.08					2.98			56.81/36.48
5:00–6:00	31.92	19.95/0	9.98					0.3	0.38/0	0.2			1.08					2.98			66.79/46.46
6:00–7:00		19.95/0	9.98	1.33					0.38/0	0.2				9				2.98			43.82/23.49
7:00–8:00		19.95/0	9.98	1.33					0.38/0	0.2				9				2.98			43.82/23.49
8:00–9:00		19.95/0	9.98	0.67					0.38/0	0.2				9				2.98			43.16/22.83
9:00–10:00		9.98/0	9.98		0.72	0.9/0	3		0.38/0	0.2					3.73	0.3	0.38/0	8.95		1.8	40.32/28.68
10:00–11:00		9.98/0	9.98		0.72	0.9/0	3		0.38/0	0.2					3.73	0.3	0.38/0	8.95		1.8	40.32/28.68
11:00–12:00		9.98/0	39.9		0.72	0.9/0	3		0.38/0	0.2	0.18	0.23/0			3.73	0.3	0.38/0	8.95		1.8	70.65/58.78
12:00–13:00		9.98/0	39.9		0.72	0.9/0	3		0.38/0	0.2	0.18	0.23/0			3.73	0.3	0.38/0	8.95		1.8	70.65/58.78
13:00–14:00		9.98/0	39.9		0.72	0.9/0	3		0.38/0	0.2	0.18	0.23/0			3.73	0.3	0.38/0	2.98	3.73		66.61/54.74
14:00–15:00		9.98/0	39.9		0.72	0.9/0	3		0.38/0	0.2	0.18	0.23/0				0.3	0.38/0	2.98	3.73		62.88/51.01
15:00–16:00		9.98/0	39.9		0.72	0.9/0	3		0.38/0	0.2	0.18	0.23/0				0.3	0.38/0	2.98	3.73		62.88/51.01
16:00–17:00		9.98/0	39.9		0.72	0.9/0	3		0.38/0	0.2	0.18	0.23/0				0.3	0.38/0	2.98	3.73		62.88/51.01
17:00–18:00		9.98/0	39.9						0.38/0	0.2	0.18	0.23/0				0.3	0.38/0	2.98	3.73		58.26/47.29
18:00–19:00	31.92	19.95/0	19.95	1.33				0.3	0.38/0	0.2	0.18	0.23/0	1.08			0.3	0.38/0	2.98			79.18/58.24

Table 1. *Cont.*

Load Sector →	Domestic Load				Community Load									Agricultural Load		Commercial Load				SIL	
					School			Hospital			Community Hall		SL	PW	MCTM	Shops		MDP	Flour Mill	Saw Mills	
Appliance →	**LED Lamp**	**Fan**	**TV + Dish**	**MC**	**LED Lamp**	**Fan**	**Computer**	**LED Lamp**	**Fan**	**Refrigerator**	**LED Lamp**	**Fan**	**LED Lights**	**Motor (2 hp)**	**Motor (5 hp)**	**LED Lamp**	**Fan**	**Motor (4 hp)**	**Motor (5 hp)**	**Saw Machine**	**Hourly Energy Demand (kWh)**
Rated Power →	**20 W**	**75 W**	**150 W**	**5 W**	**20 W**	**75 W**	**250 W**	**20 W**	**75 W**	**200 W**	**20 W**	**75 W**	**40 W**	**1.5 KW**	**3.73 kW**	**20 W**	**75 W**	**2.983kW**	**3.73kW**	**1.8kW**	
Quantity →	**2**	**1**	**1**	**1**	**12**	**12**	**12**	**5**	**5**	**1**	**3**	**3**	**27**	**6**	**1**	**5**	**5**	**3**	**1**	**1**	
19:00–20:00	31.92	19.95/0	19.95	1.33				0.3	0.38/0	0.2	0.18	0.23/0	1.08			0.3	0.38/0	2.98			79.18/58.24
20:00–21:00	31.92	19.95/0	19.95	0.67				0.3	0.38/0	0.2			1.08					2.98			77.43/57.1
21:00–22:00	31.92	19.95/0	19.95	0.67				0.3	0.38/0	0.2			1.08					2.98			77.43/57.1
22:00–23:00	15.96	19.95/0	9.98	0.67				0.3	0.38/0	0.2			1.08					2.98			51.5/31.17
23:00–24:00		19.95/0						0.3	0.38/0	0.2			1.08					2.98			24.89/4.56

SIL = Small Industrial Load; PW = Pumping Water; S/W = Summer/Winter; SL = Street Lighting; MC = Mobile Charger; MDP = Mini Diary Plant; MCTM = Multi-Crop Threshing Machine.

Table 2. MPRAMC-based scenario load demand for both winter and summer seasons.

Load Sector →	**Domestic Load**				**Community Load**									**Agricultural Load**		**Commercial Load**				**SIL**	
					School			**Hospital**			**Community Hall**		**SL**	**PW**	**MCTM**	**Shops**		**MDP**	**Flour Mill**	**Saw Mills**	
Appliance →	**LED Lamp**	**Fan**	**TV + Dish**	**MC**	**LED Lamp**	**Fan**	**Computer**	**LED Lamp**	**Fan**	**Refrigerator**	**LED Lamp**	**Fan**	**LED Lights**	**Motor (2 hp)**	**Motor (5 hp)**	**LED Lamp**	**Fan**	**Motor (4 hp)**	**Motor (5 hp)**	**Saw Machine**	**Hourly Energy Demand (kWh)**
Rated Power →	**20 W**	**75 W**	**100 W**	**5 W**	**20 W**	**75 W**	**250 W**	**20 W**	**75 W**	**200 W**	**20 W**	**75 W**	**40 W**	**1.5 kW**	**3.73 kW**	**20 W**	**75 W**	**2.983 kW**	**3.73 kW**	**1.8 kW**	
Quantity →	**2**	**1**	**1**	**1**	**12**	**12**	**12**	**5**	**5**	**1**	**3**	**3**	**27**	**6**	**1**	**5**	**5**	**3**	**1**	**1**	
Time (h) ↓		S/W				S/W			S/W			S/W					S/W				S/W
0:00–1:00		16.49/0						0.09	0.31/0	0.2			0.59					2.98			20.66/3.86
1:00–2:00		16.49/0						0.09	0.31/0	0.2			0.59					2.98			20.66/3.86
2:00–3:00		16.49/0						0.09	0.31/0	0.2			0.59					2.98			20.66/3.86
3:00–4:00		16.49/0						0.09	0.31/0	0.2			0.59					2.98			20.66/3.86
4:00–5:00	9.58	16.49/0						0.09	0.31/0	0.2			0.59					2.98			30.24/13.44
5:00–6:00	9.58	16.49/0	6.65					0.09	0.31/0	0.2			0.59					2.98			36.89/20.09
6:00–7:00		16.49/0	6.65	1.33					0.31/0	0.2				9				2.98			36.96/20.16
7:00–8:00		16.49/0	6.65	1.33					0.31/0	0.2				9				2.98			36.96/20.16
8:00–9:00		16.49/0	6.65	0.67					0.31/0	0.2				9				2.98			36.3/19.5
9:00–10:00		8.25/0	6.65		0.22	0.74/0	3		0.31/0	0.2					3.73	0.09	0.31/0	8.95		1.8	34.25/24.64
10:00–11:00		8.25/0	6.65		0.22	0.74/0	3		0.31/0	0.2					3.73	0.09	0.31/0	8.95		1.8	34.25/24.64
11:00–12:00		8.25/0	26.6		0.22	0.74/0	3		0.31/0	0.2	0.05	0.19/0			3.73	0.09	0.31/0	8.95		1.8	54.44/44.64
12:00–13:00		8.25/0	26.6		0.22	0.74/0	3		0.31/0	0.2	0.05	0.19/0			3.73	0.09	0.31/0	8.95		1.8	54.44/44.64
13:00–14:00		8.25/0	26.6		0.22	0.74/0	3		0.31/0	0.2	0.05	0.19/0			3.73	0.09	0.31/0	2.98	3.73		50.4/40.6
14:00–15:00		8.25/0	26.6		0.22	0.74/0	3		0.31/0	0.2	0.05	0.19/0				0.09	0.31/0	2.98	3.73		46.67/36.87
15:00–16:00		8.25/0	26.6		0.22	0.74/0	3		0.31/0	0.2	0.05	0.19/0				0.09	0.31/0	2.98	3.73		46.67/36.87
16:00–17:00		8.25/0	26.6		0.22	0.74/0	3		0.31/0	0.2	0.05	0.19/0				0.09	0.31/0	2.98	3.73		46.67/36.87
17:00–18:00		8.25/0	26.6						0.31/0	0.2	0.05	0.19/0				0.09	0.31/0	2.98	3.73		42.71/33.65
18:00–19:00	9.58	16.49/0	13.3	1.33				0.09	0.31/0	0.2	0.05	0.19/0	0.59			0.09	0.31/0	2.98			45.51/28.21

Table 2. *Cont.*

Load Sector →	Domestic Load				Community Load									Agricultural Load		Commercial Load				SIL	
					School			Hospital			Community Hall		SL	PW	MCTM	Shops		MDP	Flour Mill	Saw Mills	
Appliance →	**LED Lamp**	**Fan**	**TV + Dish**	**MC**	**LED Lamp**	**Fan**	**Computer**	**LED Lamp**	**Fan**	**Refrigerator**	**LED Lamp**	**Fan**	**LED Lights**	**Motor (2 hp)**	**Motor (5 hp)**	**LED Lamp**	**Fan**	**Motor (4 hp)**	**Motor (5 hp)**	**Saw Machine**	**Hourly Energy Demand (kWh)**
Rated Power →	**20 W**	**75 W**	**100 W**	**5 W**	**20 W**	**75 W**	**250 W**	**20 W**	**75 W**	**200 W**	**20 W**	**75 W**	**40 W**	**1.5 kW**	**3.73 kW**	**20 W**	**75 W**	**2.983 kW**	**3.73 kW**	**1.8 kW**	
Quantity →	**2**	**1**	**1**	**1**	**12**	**12**	**12**	**5**	**5**	**1**	**3**	**3**	**27**	**6**	**1**	**5**	**5**	**3**	**1**	**1**	
19:00–20:00	9.58	16.49/0	13.3	1.33				0.09	0.31/0	0.2	0.05	0.19/0	0.59			0.09	0.31/0	2.98			45.51/28.21
20:00–21:00	9.58	16.49/0	13.3	0.67				0.09	0.31/0	0.2			0.59					2.98			44.21/27.41
21:00–22:00	9.58	16.49/0	13.3	0.67				0.09	0.31/0	0.2			0.59					2.98			44.21/27.41
22:00–23:00	4.79	16.49/0	6.65	0.67				0.09	0.31/0	0.2			0.59					2.98			32.77/15.97
23:00–24:00		16.49/0						0.09	0.31/0	0.2			0.59					2.98			20.66/3.86

SIL = Small Industrial Load; PW = Pumping Water; S/W = Summer/Winter; SL = Street Lighting; MC = Mobile Charger; MDP = Mini Diary Plant; MCTM = Multi-Crop Threshing Machine.

Table 3. LPRAHC-based scenario load demand for both winter and summer seasons.

Load Sector →	**Domestic Load**				**Community Load**									**Agricultural Load**		**Commercial Load**				**SIL**	
	School				**Hospital**						**Community Hall**		**SL**	**PW**	**MCTM**	**Shops**		**MDP**	**Flour Mill**	**Saw Mills**	
Appliance →	**LED Lamp**	**Fan**	**TV + Dish**	**MC**	**LED Lamp**	**Fan**	**Computer**	**LED Lamp**	**Fan**	**Refrigerator**	**LED Lamp**	**Fan**	**LED Lights**	**Motor (2 hp)**	**Motor (5 hp)**	**LED Lamp**	**Fan**	**Motor (4 hp)**	**Motor (5 hp)**	**Saw Machine**	**Hourly Energy Demand (kWh)**
Rated Power →	**20 W**	**75 W**	**100 W**	**5 W**	**20 W**	**75 W**	**250 W**	**20 W**	**75 W**	**200 W**	**20 W**	**75 W**	**40 W**	**1.5 kW**	**3.73 kW**	**20 W**	**75 W**	**2.983 kW**	**3.73 kW**	**1.8 kW**	
Quantity →	**2**	**1**	**1**	**1**	**12**	**12**	**12**	**5**	**5**	**1**	**3**	**3**	**27**	**6**	**1**	**5**	**5**	**3**	**1**	**1**	
Time (h) ↓		S/W				S/W			S/W			S/W					S/W				S/W
0:00–1:00		12.77/0						0.04	0.24/0	0.2			0.35					2.98			16.58/3.57
1:00–2:00		12.77/0						0.04	0.24/0	0.2			0.35					2.98			16.58/3.57
2:00–3:00		12.77/0						0.04	0.24/0	0.2			0.35					2.98			16.58/3.57
3:00–4:00		12.77/0						0.04	0.24/0	0.2			0.35					2.98			16.58/3.57
4:00–5:00	4.26	12.77/0						0.04	0.24/0	0.2			0.35					2.98			20.84/7.83
5:00–6:00	4.26	12.77/0	6.65					0.04	0.24/0	0.2			0.35					2.98			27.49/14.48
6:00–7:00		12.77/0	6.65	1.33					0.24/0	0.2				9				2.98			33.17/20.16
7:00–8:00		12.77/0	6.65	1.33					0.24/0	0.2				9				2.98			33.17/20.16
8:00–9:00		12.77/0	6.65	0.67					0.24/0	0.2				9				2.98			32.51/19.5
9:00–10:00		6.38/0	6.65		0.1	0.58/0	3		0.24/0	0.2					3.73	0.04	0.24/0	8.95		1.8	31.91/24.47
10:00–11:00		6.38/0	6.65		0.1	0.58/0	3		0.24/0	0.2					3.73	0.04	0.24/0	8.95		1.8	31.91/24.47
11:00–12:00		6.38/0	26.6		0.1	0.58/0	3		0.24/0	0.2	0.02	0.14/0			3.73	0.04	0.24/0	8.95		1.8	52.02/44.44
12:00–13:00		6.38/0	26.6		0.1	0.58/0	3		0.24/0	0.2	0.02	0.14/0			3.73	0.04	0.24/0	8.95		1.8	52.02/44.44
13:00–14:00		6.38/0	26.6		0.1	0.58/0	3		0.24/0	0.2	0.02	0.14/0			3.73	0.04	0.24/0	2.98	3.73		47.98/40.4
14:00–15:00		6.38/0	26.6		0.1	0.58/0	3		0.24/0	0.2	0.02	0.14/0				0.04	0.24/0	2.98	3.73		44.25/36.67
15:00–16:00		6.38/0	26.6		0.1	0.58/0	3		0.24/0	0.2	0.02	0.14/0				0.04	0.24/0	2.98	3.73		44.25/36.67
16:00–17:00		6.38/0	26.6		0.1	0.58/0	3		0.24/0	0.2	0.02	0.14/0				0.04	0.24/0	2.98	3.73		44.25/36.67
17:00–18:00		6.38/0	26.6						0.24/0	0.2	0.02	0.14/0				0.04	0.24/0	2.98	3.73		40.57/33.57

Table 3. *Cont.*

Load Sector →	Domestic Load				Community Load									Agricultural Load		Commercial Load				SIL	Hourly Energy Demand (kWh)
					School			Hospital			Community Hall		SL	PW	MCTM	Shops		MDP	Flour Mill	Saw Mills	
Appliance →	LED Lamp	Fan	TV + Dish	MC	LED Lamp	Fan	Computer	LED Lamp	Fan	Refrigerator	LED Lamp	Fan	LED Lights	Motor (2 hp)	Motor (5 hp)	LED Lamp	Fan	Motor (4 hp)	Motor (5 hp)	Saw Machine	
Rated Power →	20 W	75 W	100 W	5 W	20 W	75 W	250 W	20 W	75 W	200 W	20 W	75 W	40 W	1.5 kW	3.73 kW	20 W	75 W	2.983 kW	3.73 kW	1.8 kW	
Quantity →	2	1	1	1	12	12	12	5	5	1	3	3	27	6	1	5	5	3	1	1	
18:00–19:00	4.26	12.77/0	13.3	1.33				0.04	0.24/0	0.2	0.02	0.14/0	0.35			0.04	0.24/0	2.98			35.91/22.52
19:00–20:00	4.26	12.77/0	13.3	1.33				0.04	0.24/0	0.2	0.02	0.14/0	0.35			0.04	0.24/0	2.98			35.91/22.52
20:00–21:00	4.26	12.77/0	13.3	0.67				0.04	0.24/0	0.2			0.35					2.98			34.81/21.8
21:00–22:00	4.26	12.77/0	13.3	0.67				0.04	0.24/0	0.2			0.35					2.98			34.81/21.8
22:00–23:00	2.13	12.77/0	6.65	0.67				0.04	0.24/0	0.2			0.35					2.98			26.03/13.02
23:00–24:00		12.77/0						0.04	0.24/0	0.2			0.35					2.98			16.58/3.57

SIL = Small Industrial Load; PW = Pumping Water; S/W = Summer/Winter; SL = Street Lighting; MC = Mobile Charger; MDP = Mini Diary Plant; MCTM = Multi-Crop Threshing Machine.

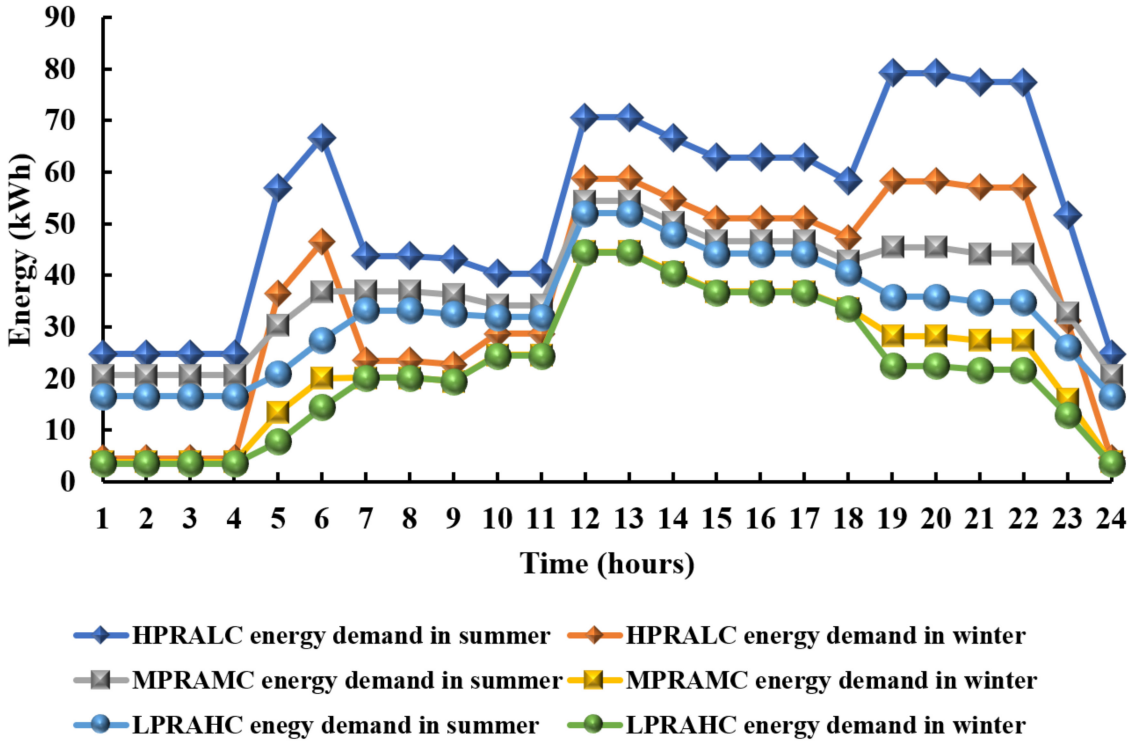

Figure 3. Hourly energy demands for all the efficient appliance usage-based scenarios in winter and summer seasons.

Taking into account the significance of the freshwater requirements, the daily requirement of the freshwater for both drinking and cooking purposes was projected as 4500 and 5000 L per day for the winter and summer seasons, respectively. Figure 4 illustrates the hourly volumetric demand of freshwater in both the winter and summer seasons.

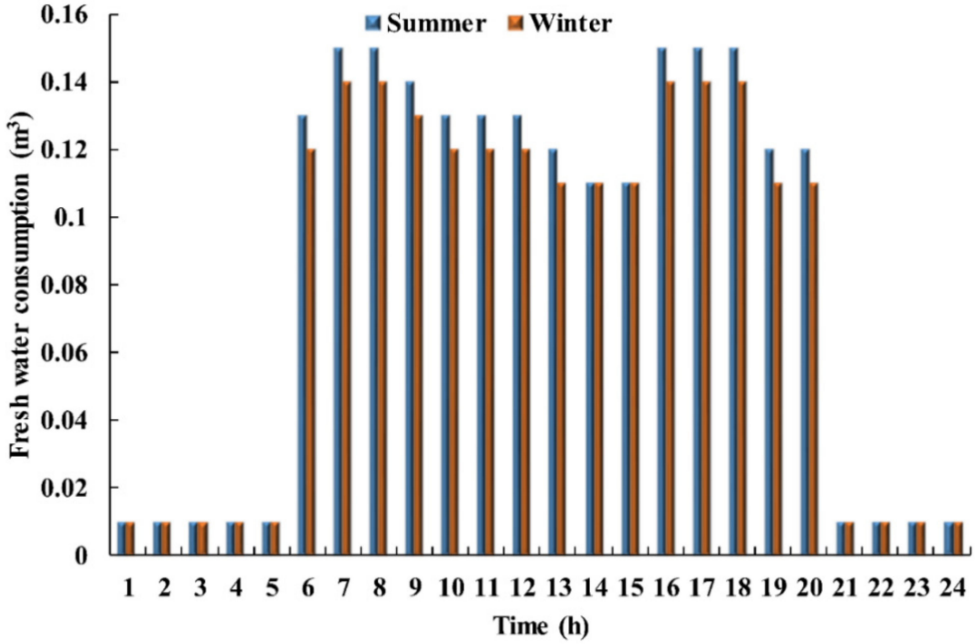

Figure 4. The volumetric hourly freshwater demand for both the winter and summer seasons.

2.3. Step 3—Resource Assessment

RE resources such as solar and biomass are abundant in the study area. It has an annual average of solar energy of 5.18 kWh/m^2/day. The annual average ambient temperature

is 26 °C. The study area is surrounded by a high dense forest covering about 87 hectares, with a collection rate of 60% of forest foliage such as leaves, pine needles, and firewood. The biomass supply is projected to be 9 tons/year. The study considered in the simulation an average of 10 years (2005–2015) of hourly solar radiation and ambient temperatures, which were taken from the National Renewable Energy Laboratory (NREL) and are shown in Figures 5 and 6.

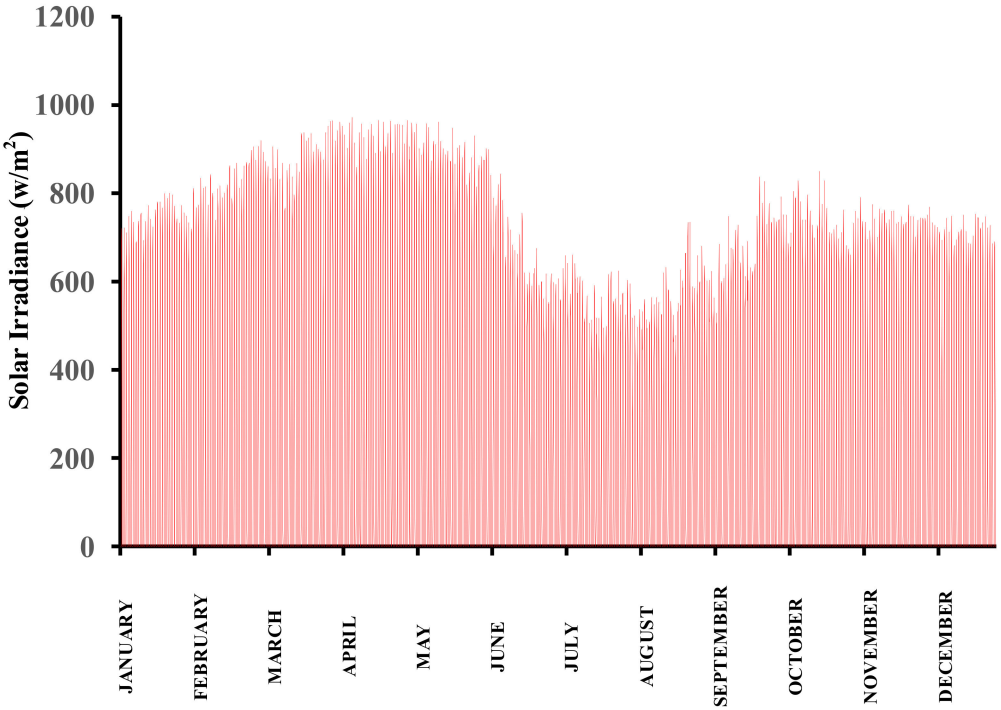

Figure 5. Annual global solar radiation of the study area.

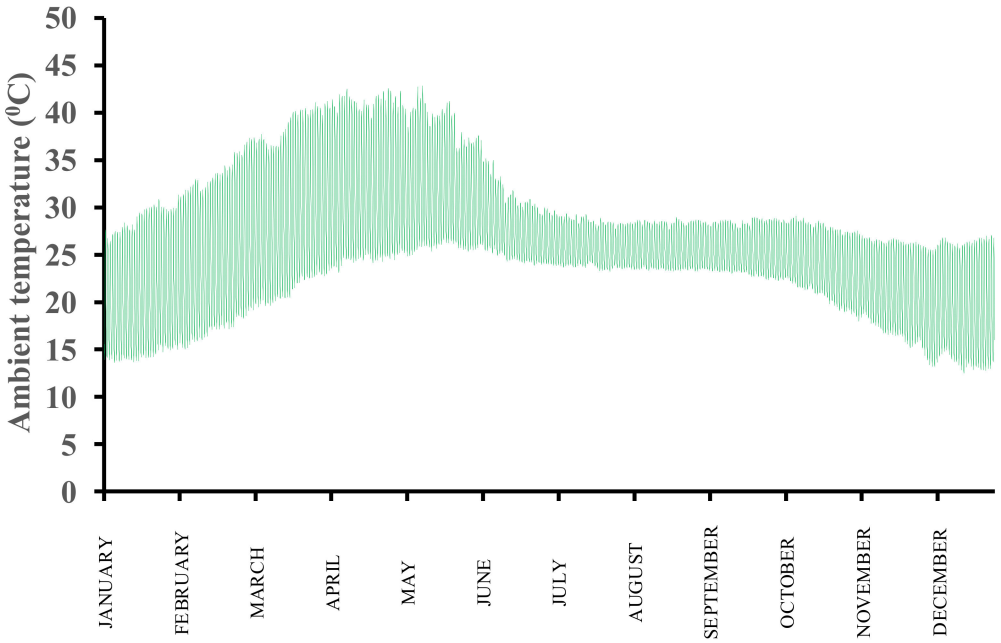

Figure 6. The annual ambient temperature of the study area.

3. The IHRES Component Mathematical Modelling

Before optimal sizing of the IHRES, proper mathematical modelling of the components is needed. The study proposed an IHRES model that incorporates biomass and solar energy

resources as well as a battery bank and diesel generator as a backup power supply. Its schematic diagram is depicted in Figure 7 and the corresponding mathematical models are described as follows.

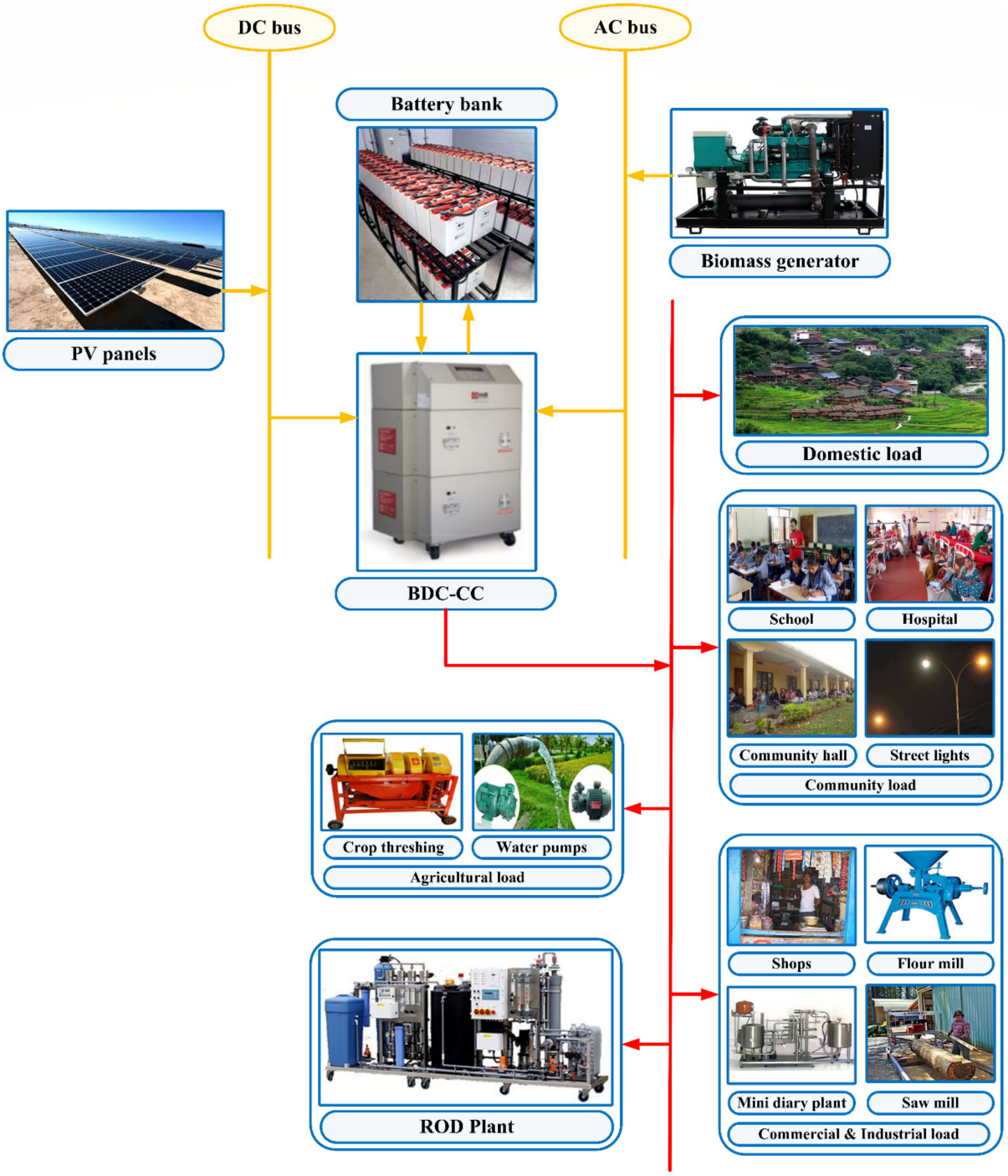

Figure 7. The schematic diagram of the IRES.

3.1. Solar Energy System

Various models for measuring PV output power have been proposed in the literature. In this analysis, a simplified model was used to calculate the output power of a PV panel

$(P_{PV}(t))$ by using Equation (1) based on the hourly ambient temperature $(T_{amb}(t))$ and hourly solar irradiation $(G(t))$ in the study area [9].

$$P_{PV}(t) = PV_{rated} \times (G(t)/G_{ref}) \times \left[1 + K_T \times \left(T_C - T_{ref}\right)\right] \quad (1)$$

where, G_{ref} is a reference condition solar radiation, its value is 1000 W/m^2, K_T is the maximum power temperature coefficient, its value is 3.7 × 10 − 3 (1/°C), T_{ref} is at the standard test condition *PV* cell temperature, its value is 25 °C, and PV_{rated} is the *PV* panel rated power.

The cell temperature (T_C) is calculated as:

$$T_C = T_{amb}(t) + (0.0256 \times G(t)). \quad (2)$$

where, $T_{amb}(t)$ is the hourly ambient temperature (°C).

The *PV* panel energy generation (E_{PV}) is calculated as follows:

$$E_{PV}(t) = N_{PV} \times P_{PV}(t) \times \Delta t \quad (3)$$

where, Δt is the time span and is considered as one hour.

3.2. Biomass Generator (BMG)

The biomass generator is made up of four major components such as "producer gas-based engine cum generator set, gas cleaning system, gas cooling system and biomass gasifier. For the biomass gasifier, the study used a downdraft gasifier design; in this gasifier, mainly seven parts are there such as drying zone, hopper lid, combustion zone, reduction zone, pyrolysis zone, ash removal tank and smoke valve. The cleaning system consists of pan filter, a cyclone, cotton filter and sawdust filter and the cooling system consists of a chiller plant" [43,44]. The front and rear views of the biomass generator are shown in Figures 8 and 9, respectively.

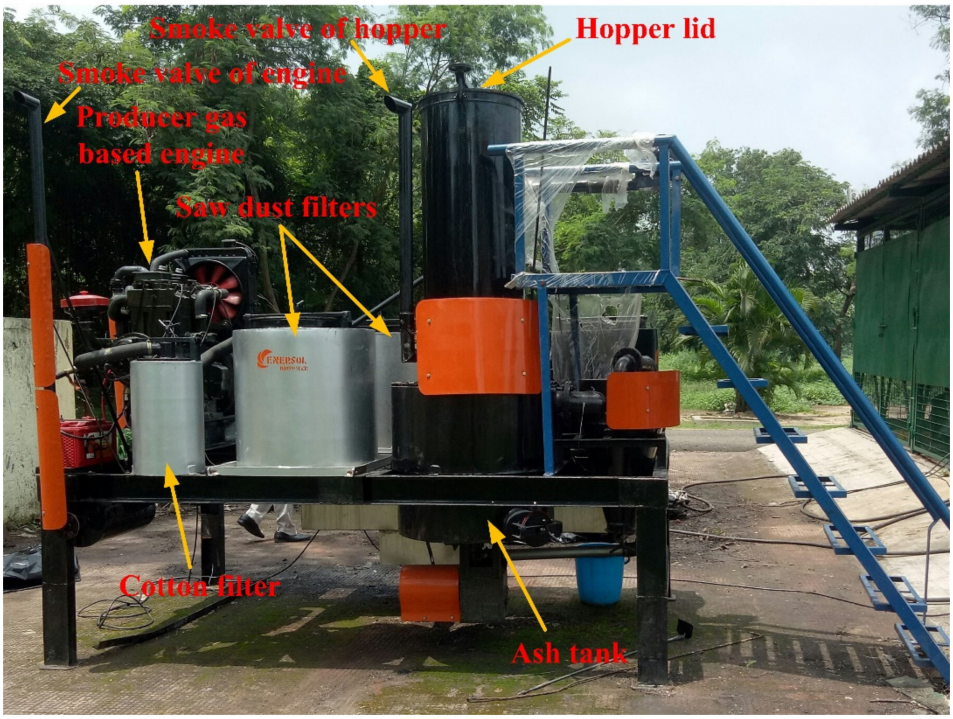

Figure 8. Front view of the biomass generator [44].

Figure 9. Rear view of the biomass generator [44].

The power generated by the biomass generator (P_{BMG}) is calculated as [14]:

$$P_{BMG}(t) = \frac{Q_{BM} \times \eta_{BMG} \times CV_{BM} \times 1000}{DOH_{BMG} \times 365 \times 860} \quad (4)$$

where, η_{BMG} is the efficiency of the *BMG*, CV_{BM} is the calorific value of the biomass, its value is 4015 kcal/kg, DOH_{BMG} is the daily operative hours of the *BMG*, the 860 value used in the formula is a converting factor from kcal to kWh, and Q_{BM} is the availability of the quantity of biomass (tons/year).

The energy generated by the *BMG* (E_{BMG}) is calculated as follows:

$$E_{BMG}(t) = P_{BMG}(t) \times \Delta t \quad (5)$$

where, Δt is the time period and is considered to be one hour.

3.3. Battery Bank

When RE resources are unavailable or the system is experiencing peak load demand, the battery bank usually supplies the power. Whenever excess energy is generated by the RE resources, it is stored in the battery bank. The energy stored in the battery bank at any hour 't' is expressed as follows [9]:

$$E_{Bat}(t) = (1 - \sigma) \times E_{Bat}(t-1) + (E_G(t) - E_L(t)/\eta_{Conv}) \times \eta_{CC} \times \eta_{rbat} \quad (6)$$

where, σ is the battery hourly self-discharge rate, E_G is the electrical energy generated, E_L is the electrical energy demand, η_{Conv} is the bi-directional converter efficiency, η_{CC} is the charge controller efficiency, η_{rbat} is the battery round trip efficiency, and $E_{Bat}(t)$ and $E_{Bat}(t-1)$ are battery bank energy levels at time 't' and '$t-1$', respectively.

The electrical energy generated (E_G) by the RE resources are calculated as follows:

$$E_G(t) = [E_{DC}(t) + E_{AC}(t)] \times \eta_{Conv} \quad (7)$$

where the *DC* energy generated (E_{DC}) by the RE resources are calculated as follows:

$$E_{DC}(t) = E_{PV}(t) \quad (8)$$

The *AC* energy generated (E_{AC}) by the RE resources are calculated as follows:

$$E_{AC}(t) = E_{BMG}(t) \tag{9}$$

The electrical power generated by the RE resources during the discharge process is less than the load demand. Therefore, the battery bank can provide the necessary deficit load, which can be expressed as follows:

$$E_{Bat}(t) = (1 - \sigma) \times E_{Bat}(t-1) - (E_L(t)/\eta_{Conv} - E_G(t))/\eta_{rbat} \tag{10}$$

3.4. Diesel Generator (DG)

Diesel generators are beneficial in off-grid areas because they provide power when batteries fail to fulfill the load demand or when renewable energy supplies are disrupted by prolonged cloudy weather or rainy seasons. The main reason for including DG in the study is that many households, primary health care centers, and businesses are left in the dark during the blackouts caused by super storms and other unexpected occurrences. Furthermore, in the last ten years, blackout cases have doubled. Thus, incorporating a DG set into integrated RE systems improves the efficiency of a microgrid by providing a reliable power source in emergency situations and sharing peak load demands when batteries fail to meet the peak load demands [45,46]. The DG hourly fuel consumption (F_{DG}) can be calculated using a linear law based on the required load demand as follows [9]:

$$F_{DG}(t) = \left(a_{DG} \times P_{DG,gen}(t) + b_{DG} \times P_{DG,rat}\right) l/h \tag{11}$$

where, a_{DG} and b_{DG} are the DG fuel consumption curve coefficients and their values are a_{DG} = 0.246 (l/kWh) and b_{DG} = 0.08145 (l/kWh). $P_{DG,gen}(t)$ and $P_{DG,rat}$ are the hourly generated power and rated power of the DG, respectively.

The DG annual fuel consumption (AFC) is calculated as follows:

$$AFC = \sum_{t=1}^{8760} F_{DG}(t) \tag{12}$$

CO_2 Emissions

The hourly CO_2 emissions of DG estimated with respect to the hourly fuel consumption are as follows [47]:

$$CO_2(t) = SE_{CO_2}(\ kg/l) \times F_{DG}(t)(\ l/h) \tag{13}$$

where, SE_{CO_2} is the specific CO_2 emissions per L of diesel and its value is 2.7 kg/L.

The DG annual CO_2 emissions are estimated as follows:

$$A_{CO_2}\ emission = \sum_{t=1}^{8760} CO_2(t) \tag{14}$$

3.5. Bi-Directional Converter with a Charge Controller (BDC-CC)

In general, the BDC-CC converts electrical energy into rectifier and inverter modes of operation. In the inverter mode, it converts the direct current (DC) into an alternate current (AC) and in the rectifier mode, it converts AC into DC. The charge controller is useful for ensuring that the battery bank is not overcharged or over-discharged. The BDC-CC power rating ($P_{BDC\text{-}CC}$) is calculated as follows [14]:

$$P_{BDC\text{-}CC} = E_{T,max} \times 1.1 \tag{15}$$

where, the multiplication factor 1.1 represents the converter's 10% overloading capability and $E_{T,max}$ is the maximum amount of energy transferred through the converter.

3.6. Reverse Osmosis Desalination (ROD) Plant

In relation to the specific energy consumption (S_{EC}), the power (P_{DEM}) required by the ROD unit to generate an hourly freshwater demand (H_{VDW}) for the desalination process is expressed as follows [1]:

$$P_{DEM}(t) = H_{VDM}(t) \times S_{EC} \tag{16}$$

In this study, the ROD unit was expected to consume 2 kWh/m^3 (S_{EC}) of specific energy. The ROD unit consists of pumps, a desalination unit, membranes, and energy recovery devices. The ROD unit's daily volumetric demand of freshwater (D_{VDW}) is calculated as follows:

$$D_{VDW} = 24 \times \left(\frac{P_{DEM}}{S_{EC}}\right) \tag{17}$$

To analyze the characteristic curves of RO membranes, the ROD system was designed to operate in between the installed power (P_I) and minimum load requirement (P_{MLD}), i.e.,

$$P_{MLD} \leq P_{DEM} \leq P_I \tag{18}$$

where, the ROD unit's minimum load demand (P_{MLD}) is used to resolve the osmotic pressure produced by the ROD unit, which was estimated to be 25% of the installed power (P_I).

The ROD unit autonomy assumes a two-day storage period of a freshwater tank to calculate the volumetric capacity of a freshwater tank (V_{CWT}), which is calculated as follows:

$$V_{CWT} = 2 \times D_{VDW} \tag{19}$$

4. Economic Analysis of the IRES

Several approaches have been used to investigate the economic feasibility of the IHRES such as net present cost, annual levelized cost, life cycle cost (LCC), and payback period. In these scenarios, the LCC methodology for economic analysis is extensively employed since it provides an accurate overview of project expenses over the project's lifespan. In this study, the LCC of the IHRES was calculated using Equation (20) [46] by summing the erection costs, initial capital costs, O&M costs, fuel costs, and replacement costs of all system components. The analysis comprised the following assumptions.

The erection costs of the PV, BMG, DG, BAT, BDC-CC, and ROD unit were taken as 20% [14], 5% [14], 5%, 3% [14], 3% [14], and 3% [46] of their capital costs, respectively.

The replacement cost of the BMG, DG, BAT, BDC-CC, MEM, and CHEM were considered as 70% [14], 100% [46], 100% [14], 100% [14], 100% [14], and 100% [14] of their capital costs, respectively.

$$LCC = ICC + P_{V,O\&M} + P_{V,REP} + P_{V,FUEL} \tag{20}$$

The initial capital cost (ICC) of the IRES components are calculated as follows [14]:

$$ICC = \begin{bmatrix} (C_{BMG,cap}) + (N_{PV} \times C_{PV,cap}) + (N_{BAT} \times C_{BAT,cap}) + \\ (C_{ROD,cap}) + (C_{BDC\text{-}CC,cap}) + (C_{MEM,cap}) + (C_{WTA,cap}) + (C_{CHE,cap}) \end{bmatrix} \tag{21}$$

where, $C_{BMG,cap}$, $C_{PV,cap}$, $C_{BAT,cap}$, $C_{ROD,cap}$, $C_{BDC\text{-}CC,cap}$, $C_{MEM,cap}$, $C_{WTA,cap}$, and $C_{CHE,cap}$ are the initial capital costs of the BMG, PV, BAT, ROD unit, BDC-CC, MEM, WTA, and CHE, respectively.

The erection costs ($EREC$) of the IRES components are calculated as follows [14]:

$$EREC = \begin{bmatrix} (N_{PV} \times C_{PV,erect}) + (C_{ROD,erect}) + \\ \left((N_{BAT} \times C_{BAT,erect}) \times \sum_{b=1}^{N_r} \frac{(1+x)^{bN_c-1}}{(1+y)^{bN_c}}\right) + \\ \left(C_{BDC\text{-}CC,erect} \times \sum_{d=1}^{N_r} \frac{(1+x)^{dN_c-1}}{(1+y)^{dN_c}}\right) + \left(C_{BMG,erect} \times \sum_{g=1}^{N_r} \frac{(1+x)^{gN_c-1}}{(1+y)^{gN_c}}\right) \end{bmatrix} \tag{22}$$

where, $C_{PV,erect}$, $C_{ROD,erect}$, $C_{BAT,erect}$, $C_{BDC\text{-}CC,erect}$, and $C_{BMG,erect}$ are erection costs of PV, ROD unit, BAT, BDC-CC, and BMG, respectively.

The present value of annual O&M ($P_{V,O\&M}$) costs of the IRES components are calculated as follows [14]:

$$P_{V,O\&M} = \begin{bmatrix} (N_{PV} \times C_{PV,o\&m}) + (C_{BMG,o\&m}) \\ (N_{BAT} \times C_{BAT,o\&m}) + (C_{BDC\text{-}CC,o\&m}) + (C_{ROD,o\&m}) \end{bmatrix} \times \sum_{i=1}^{N} \frac{(1+x)^{i-1}}{(1+y)^{i}} \quad (23)$$

where, $C_{PV,o\&m}$, $C_{BMG,o\&m}$, $C_{BAT,o\&m}$, $C_{BDC\text{-}CC,o\&m}$, and $C_{ROD,o\&m}$ are O&M costs of the PV, BMG, BAT, BDC-CC, and ROD unit, respectively, and y is defined as follows [14]:

$$y = \frac{I_{nom} - x}{1 + x} \quad (24)$$

where, I_{nom}, y, N, and x are the nominal interest rate, discount rate, lifespan, and the inflation rate of the project, respectively.

The components' lifespan such as that of batteries, biomass generator, bi-directional converter with a charge controller, membranes, chemicals, and DG are shorter than the project lifetime. Therefore, they need to be replaced at some stage during the project's lifetime. The present value of annual replacement cost ($P_{V,REP}$) of the IRES is calculated as follows:

$$P_{V,REP} = \begin{bmatrix} \left(N_{BAT} \times C_{BAT,rep} \times \sum_{b=1}^{N_r} \frac{(1+x)^{bN_c-1}}{(1+y)^{bN_c}}\right) + \left(C_{BMG,rep} \times \sum_{g=1}^{N_r} \frac{(1+x)^{gN_c-1}}{(1+y)^{gN_c}}\right) + \\ \left(C_{CHE,rep} \times \sum_{c=1}^{N_r} \frac{(1+x)^{cN_c-1}}{(1+y)^{cN_c}}\right) + \left(C_{BDC\text{-}CC,rep} \times \sum_{d=1}^{N_r} \frac{(1+x)^{dN_c-1}}{(1+y)^{dN_c}}\right) + \\ \left(N_{MEM} \times C_{MEM,rep} \times \sum_{i=1}^{N_r} \frac{(1+x)^{mN_c-1}}{(1+y)^{mN_c}}\right) \end{bmatrix} \quad (25)$$

where, $C_{BAT,rep}$, $C_{BMG,rep}$, $C_{CHE,rep}$, $C_{BDC\text{-}CC,rep}$, and $C_{MEM,rep}$ are the replacement costs of the BAT, BMG, CHE, BDC-CC, and MEM, respectively, and the N_r is defined as follows [14]:

$$N_r = int\left(\frac{N - N_c}{N_c}\right) \quad (26)$$

where, N_r and N_c are the number of replacements needed for the system components and lifespan of each system component, respectively.

The present value of annual fuel cost ($P_{V,FUEL}$) of the IRES is calculated as [14]:

$$P_{V,FUEL} = [(C_{BM} \times Q_{BM}) + (AFC_{DG})] \times \sum_{i=1}^{N} \frac{(1+x)^{i-1}}{(1+y)^{i}} \quad (27)$$

where C_{BM} and Q_{BM} are the cost and quantity of the biomass, respectively, and AFC_{DG} is the annual fuel consumption of the DG.

5. The Objective Function and Its Constraints

The system's objective function, i.e., life cycle cost (LCC), and its constraints are discussed as follows.

5.1. Life Cycle Cost

The objective function as expressed in Equation (28) was used to calculate the system's life cycle cost. The objective function is primarily dependent on two integer decision variables such as the number of batteries (N_{BAT}) and PV panels (N_{PV}).

$$min\ LCC(N_{PV}, N_{BAT}) = \sum_{C=PV,BMG,BAT,ROD,BDC-CC}^{min} (LCC)_C \tag{28}$$

5.2. Upper and Lower Bounds

In this study, it was presumed that the biomass generator operates as a fixed energy resource with a rated power of 5 kW and works daily for five hours during the peak load demands, i.e., from 6 P.M. to 10 P.M., to generate 4 kWh of energy per hour. Hence, it was not bound by any constraints. Furthermore, the remaining solar energy resource was subject to the following constraint.

$$0 \leq N_{PV} \leq N_{PV-max} \tag{29}$$

where, N_{PV} is the number of PV panels.

Furthermore, the battery bank was subjected to the following constraint.

$$0 \leq N_{BAT} \leq N_{BAT-max} \tag{30}$$

where, N_{BAT} is the number of batteries.

5.3. Battery Bank Energy Storage Limits

The amount of energy stored in the battery bank at any hour 't' is determined by the following constraint [45]:

$$E_{Bat\_min} \leq E_{Bat}(t) \leq E_{Bat\_max} \tag{31}$$

The maximum and minimum energy storage levels of the battery bank is calculated as follows:

$$E_{Bat\_max} = \left(\frac{N_{BAT} \times V_{BAT} \times S_{BAT}}{1000}\right) \times SOC_{max-bat} \tag{32}$$

$$E_{Bat\_min} = \left(\frac{N_{BAT} \times V_{BAT} \times S_{BAT}}{1000}\right) \times SOC_{min-bat} \tag{33}$$

where, V_{BAT} and S_{BAT} are the voltage and rated capacity (Ah) of the battery, respectively.

The minimum and maximum state of charges of the battery is calculated as follows:

$$SOC_{min-bat} = 1 - DOD$$

$$SOC_{max-bat} = SOC_{min-bat} + DOD$$

where, DOD is the depth of discharge of the battery.

5.4. Diesel Generator Operating Limits

At higher loads, the diesel generator is much more efficient. As a result, the minimum load required for the DG operation is set at 40% of its rated capacity. Accordingly, the DG runs in the operating mode after adhering to the limitations mentioned below [48]:

$$\frac{E_L(t)}{\eta_{conv}} \geq 40\% \text{ of } P_{rdg} \times \Delta t \tag{34}$$

where $E_L(t)$ is the hourly energy demand, η_{conv} is the efficiency of the converter, P_{rdg} is the rated power of the diesel generator, and Δt is the time period.

5.5. Power Reliability Index

The power system's reliability is described as its ability to supply power for a specified period of time under specific conditions. In this study, The IHRES power reliability was assessed using the loss of power supply probability (LPSP), which is calculated by summing the hours of a power outage to the sum of hourly energy demands. The loss of power supply (*LPS*) at any hour '*t*' is calculated as follows [1]:

$$LPS(t) = \frac{E_L(t)}{\eta_{Conv}} - E_G(t) - [(1-\sigma) \times E_{Bat}(t-1) - E_{Bat\_min}] \times \eta_{rbat} \quad (35)$$

The *LPSP* is calculated as follows [1]:

$$LPSP = \frac{\sum_{t=1}^{T} LPS(t)}{\sum_{t=1}^{T} E_L(t)} \quad (36)$$

During the optimization process, the following constraint is useful for analyzing the maximum permissible loss of power supply probability (*LPSP**).

$$LPSP^* \geq LPSP \quad (37)$$

6. Methodology

6.1. Load following Strategy

The main feature of the LF strategy is that the DG can satisfy the deficiency load demand when the batteries and RE resources are unable to supply the electricity demand. The key concern is that it just provides the deficit load demand only and does not charge the batteries. The overall operation of the LF strategy is outlined in the following modes [24].

6.2. Cycle Charging Strategy

The CC strategy is distinguished by the fact that the DG turns on to satisfy the deficit load demand while also storing energy in the battery bank through the charging process. The overall operation of the CC strategy is outlined in the following modes [49]:

The complete EMS operation was conducted in the MATLAB© environment by simulating the input parameters such as techno-economic values of the components, load demand, ambient temperature, and solar irradiation for 8760 h, i.e., for 1 year.

The system's electrical energy demand at any hour '*t*' is determined as follows:

$$E_L(t) = (E_{Load}(t) + E_{ROD}(t))/\eta_{Conv} \quad (38)$$

The electricity provided by the RE resources (E_G) is computed at any hour '*t*' as follows:

$$E_G(t) = [E_{DC}(t) + E_{AC}(t)] \times \eta_{Conv} \quad (39)$$

where the generated AC energy (E_{AC}) and DC energy (E_{DC}) are calculated as follows:

$$E_{DC}(t) = E_{PV}(t) \quad (40)$$

$$E_{AC}(t) = E_{BMG}(t) \quad (41)$$

During the peak load time from 6 P.M. to 10 P.M., the biomass generator works daily. The minimum and maximum battery bank energy storage limits are calculated as follows:

$$E_{Bat\_min} = \left(\frac{N_{BAT} \times V_{BAT} \times S_{BAT}}{1000}\right) \times SOC_{min-bat} \quad (42)$$

$$E_{Bat\_max} = \left(\frac{N_{BAT} \times V_{BAT} \times S_{BAT}}{1000}\right) \times SOC_{max-bat} \quad (43)$$

where, S_{BAT} and V_{BAT} are the rated capacity (Ah) and voltage of the battery, respectively.

The minimum and maximum state of charge (SOC) of the battery bank are estimated as follows:

$$SOC_{max-bat} = SOC_{min-bat} + DOD \tag{44}$$

$$SOC_{min-bat} = 1 - DOD \tag{45}$$

where, *DOD* is the depth of discharge of the batteries.

At any hour '*t*', the net energy of the system is estimated as the difference between the hourly energy generated by the RE resources and the projected load demand:

$$E_{net}(t) = E_G(t) - E_L(t) \tag{46}$$

Now, the 'for' loop begins for 8760 h of simulation.

For t = 1:8760

$$\text{if } E_{net}(t) = 0 \tag{47}$$

Mode 1: in this operating mode, the total net energy provided by the system is equal to 0, and the energy level of the battery bank at that time 't' is equal to the energy level of the previous hour. This mode of operation is described pictorially in Figure 10a, which explains that the switches S_1 and S_3 are in the closed position and the switches S_2, S_4, and S_5 are in the open position. The expected load demand is met and there is no power outage, which is mathematically expressed as follows:

$$E_{Bat}(t) = E_{Bat}(t-1) \tag{48}$$

$$LPS(t) = 0 \tag{49}$$

$$E_{Load\_supplied}(t) = E_L(t) \tag{50}$$

$$\text{elseif } E_{net}(t) > 0 \tag{51}$$

$$E_{ch}(t) = E_G(t) - E_L(t) \tag{52}$$

$$\text{if } E_{ch}(t) \leq E_{Bat\_max} - E_{Bat}(t-1) \tag{53}$$

Mode 2: in this operating mode, the RE resources first meet the load demand and then store the produced surplus energy in the battery bank if the energy levels in the battery bank are between the minimum and maximum range, i.e., if $(E_{Bat\_min} \leq E_{Bat}(t) \leq E_{Bat\_max})$. This mode of operation is described pictorially in Figure 10b, which explains that the switches S_1, S_2, and S_3 are in the closed position and the switches S_4 and S_5 are in the open position. The expected load demand is met and there is no power outage, which is mathematically expressed as follows:

$$E_{Bat}(t) = (1-\sigma) * E_{Bat}(t-1) + E_{ch}(t) * \eta_{CC} * \eta_{rbat} \tag{54}$$

$$LPS(t) = 0 \tag{55}$$

$$E_{Load\_supplied}(t) = E_L(t) \tag{56}$$

$$\text{else}$$

Mode 3: in this operating mode, energy from the RE resources initially satisfies the load demand, and if the energy level of the battery bank is at its maximum limit, i.e., if $(E_{Bat}(t) = E_{Bat\_max})$, then the surplus energy is used to operate the dump load. In this mode of operation, as shown in Figure 10c, S_1, S_3, and S_5 switches are in a closed position and S_2 and S_4 switches are in an open position. The expected load demand is met and there is no power outage, which is mathematically expressed as follows:

$$E_{Bat}(t) = E_{Bat\_max} \tag{57}$$

$$LPSP^{*} \geq LPSP \tag{58}$$

$$E_{dump}(t) = E_{ch}(t) - (E_{Bat\_max} - E_{Bat}(t-1)) \tag{59}$$

$$LPS(t) = 0 \tag{60}$$

$$E_{Load\_supplied}(t) = E_{L}(t) \tag{61}$$

end

elseif $E_{net}(t) < 0$

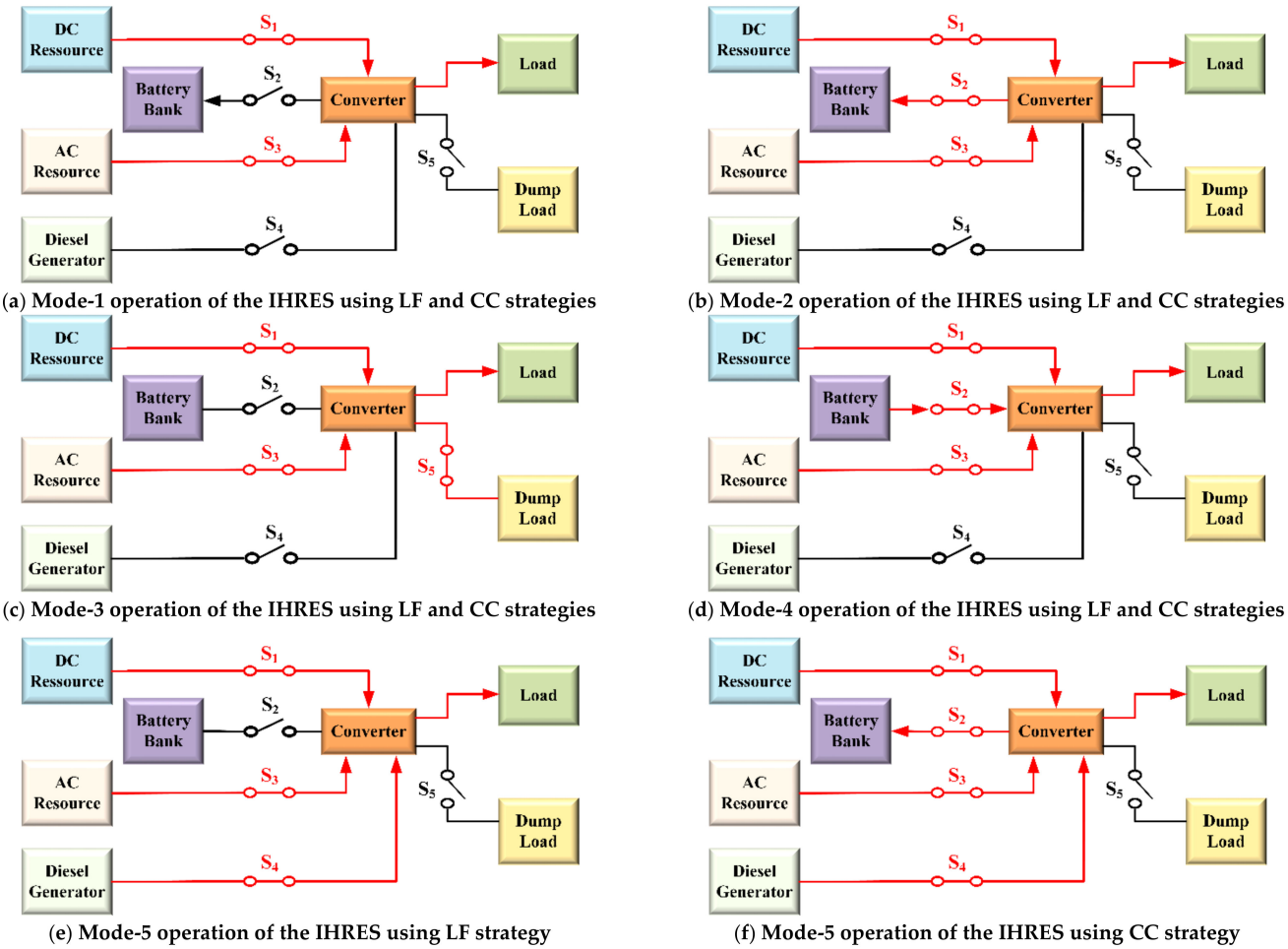

(a) Mode-1 operation of the IHRES using LF and CC strategies

(b) Mode-2 operation of the IHRES using LF and CC strategies

(c) Mode-3 operation of the IHRES using LF and CC strategies

(d) Mode-4 operation of the IHRES using LF and CC strategies

(e) Mode-5 operation of the IHRES using LF strategy

(f) Mode-5 operation of the IHRES using CC strategy

Figure 10. Operating modes of the IRES using LF and CC strategies.

Mode 4: in this operating mode, the energy provided by the RE resources is less than the load requirement, so the battery bank provides the deficit load demand; if $(E_{Bat}(t) \geq E_{Bat\_max})$. In this mode of operation, as shown in Figure 10d, S_1, S_2, and S_3 switches are in a closed position and S_4 and S_5 switches are in an open position. The expected load demand is met and there is no power outage, which is mathematically expressed as follows:

$$E_{dch}(t) = E_{L}(t) - E_{G}(t) \tag{62}$$

$$\text{If } (E_{Bat}(t-1) - E_{Bat\_min}) \geq E_{dch}(t) \tag{63}$$

$$E_{Bat}(t) = (1-\sigma) \times E_{Bat}(t-1) - E_{dch}(t)/\eta_{rbat} \tag{64}$$

$$LPS(t) = 0 \tag{65}$$

$$E_{Load\_supplied}(t) = E_{L}(t) \tag{66}$$

$$\text{elseif } \frac{E_L(t)}{\eta_{conv}} \geq 40\% \text{ of } P_{rdg} \times \Delta t \tag{67}$$

If the system operates with the LF strategy.

Mode 5: if the energy provided by the RE resources and the battery bank is insufficient to meet the load demand, then the DG is operational in order to satisfy the deficit load demand if $(E_{Bat}(t) \leq E_{Bat\_min})$. The DG comes to a halt when the RE resources begin to produce enough power to meet the full load requirements. In this mode of operation, as shown in Figure 10e, S_1, S_3, and S_4 switches are in a closed position and S_2 and S_5 switches are in an open position. The expected load demand is met and there is no power outage, which is mathematically expressed as follows:

$$E_{Bat}(t) = E_{Bat\_min} \tag{68}$$

$$LPS(t) = E_L(t) - E_G(t) \tag{69}$$

$$E_{Load\_supplied}(t) = E_G(t) \tag{70}$$

(or)

If the system operates with the CC strategy.

Mode 5: if the energy provided by the RE resources and the battery bank is insufficient to meet the load demand, the DG operates at its rated capacity to meet the load demand while also charging the battery bank, if $(E_{Bat}(t) \leq E_{Bat\_max})$. When the RE resources provide enough power to fulfil the full load requirements, the DG comes to a halt. In this mode of operation, as shown in Figure 10f, S_1, S_2, S_3, and S_4 switches are in a closed position and the S_5 switch is in an open position. The expected load demand is met and there is no power outage, which is mathematically expressed as follows:

$$E_{DG}(t) = P_{DG,rat} * \Delta t \tag{71}$$

$$F_{DG}(t) = \left(a_{DG} * P_{DG,gen}(t) + b_{DG} * P_{DG,rat}\right) l/h \tag{72}$$

$$LPS(t) = 0 \tag{73}$$

$$E_{Bat}(t) = (1 - \sigma) * E_{Bat}(t-1) + E_{ch}(t) * \eta_{CC} * \eta_{rbat} \tag{74}$$

$$E_{Load\_supplied}(t) = E_L(t) \tag{75}$$

Else

Mode 6: in this operating mode, the energy provided by the RE resources is less than the required load demand and the energy level of the battery bank is also less than the prescribed minimum level, i.e., $E_{Bat}(t) = E_{Bat\_min}$, so at that time '*t*', there is a loss of power supply, which is mathematically expressed as follows:

$$E_{Bat}(t) = E_{Bat\_min} \tag{76}$$

$$LPS(t) = E_L(t) - E_G(t) \tag{77}$$

$$E_{Load\_supplied}(t) = E_G(t) \tag{78}$$

end

end

end (end of for loop)

The system's LPSP can now be determined by dividing the cumulative loss of power supply hours by the annual load demand which is described as follows:

$$LPSP = \frac{\sum_{t=1}^{T} LPS(t)}{\sum_{t=1}^{T} E_L(t)} \tag{79}$$

The operating modes of the IHRES using LF and CC strategies are pictorially shown in Figure 10.

Figures 11–13 represent a flowchart of the aforementioned EMS operating modes as well as the acquisition of LPSP.

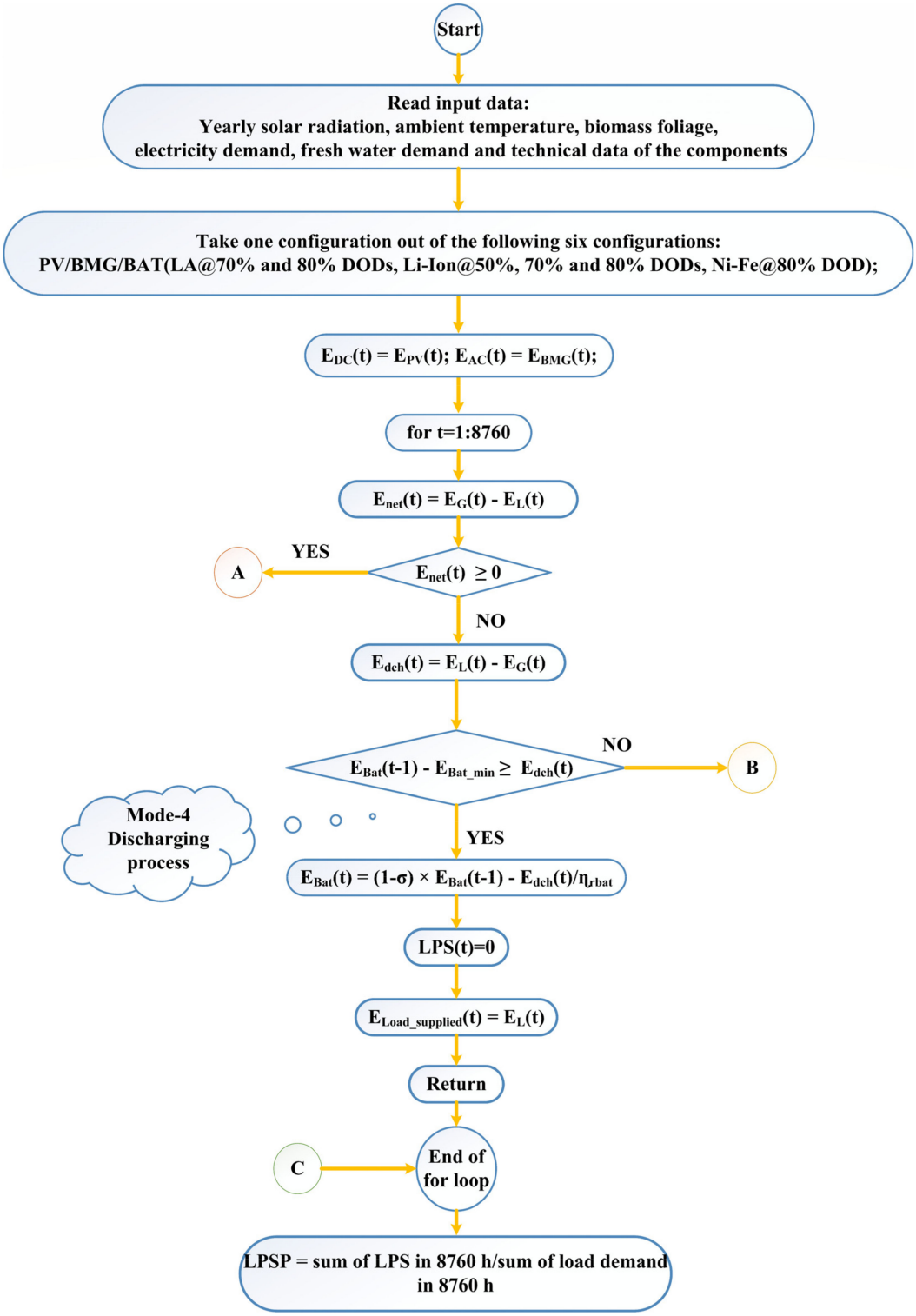

Figure 11. Flowchart of the EMS operating modes and acquisition of LPSP using LF and CC strategies.

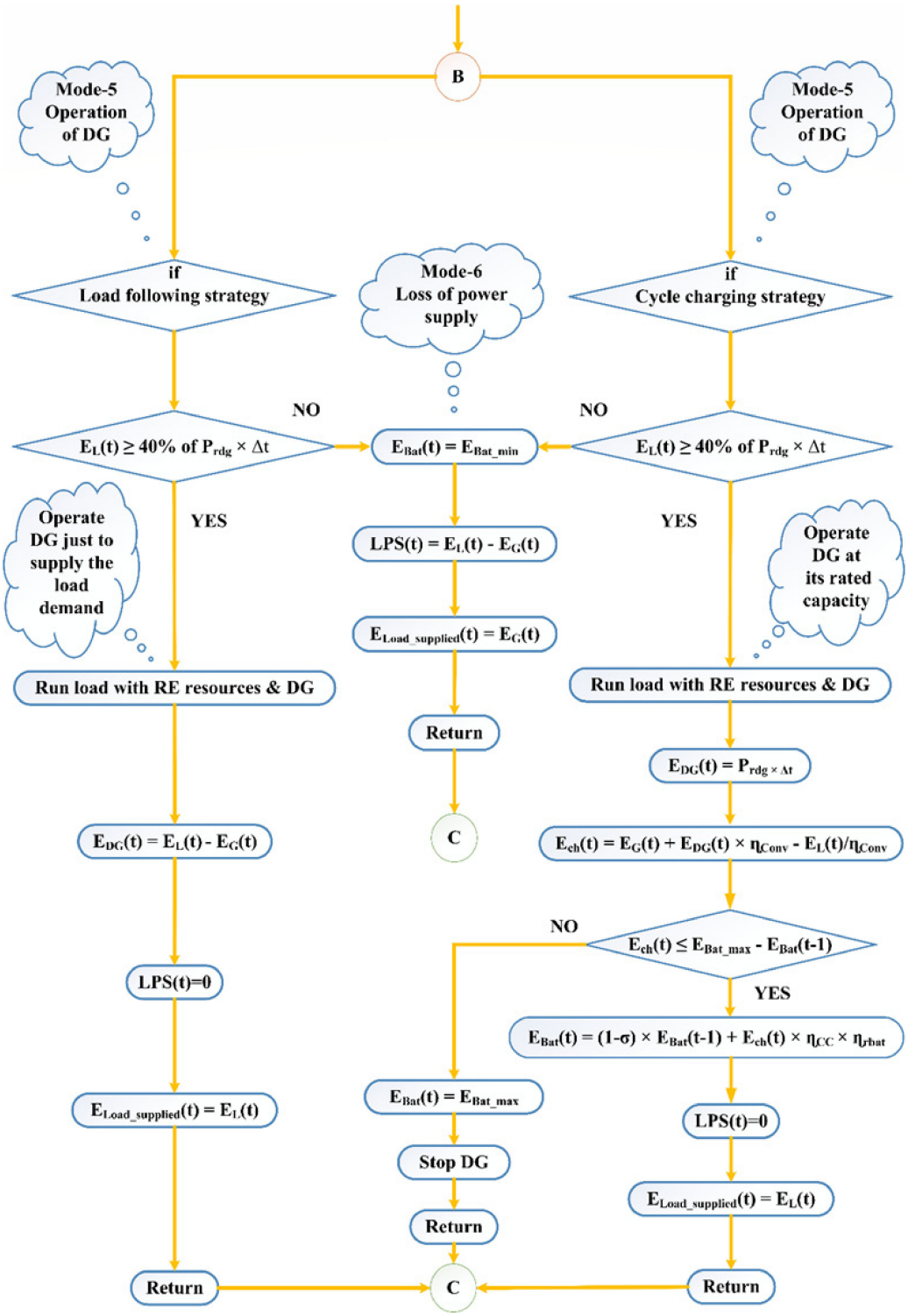

Figure 12. Flowchart of the EMS operating modes and acquisition of LPSP using LF and CC strategies.

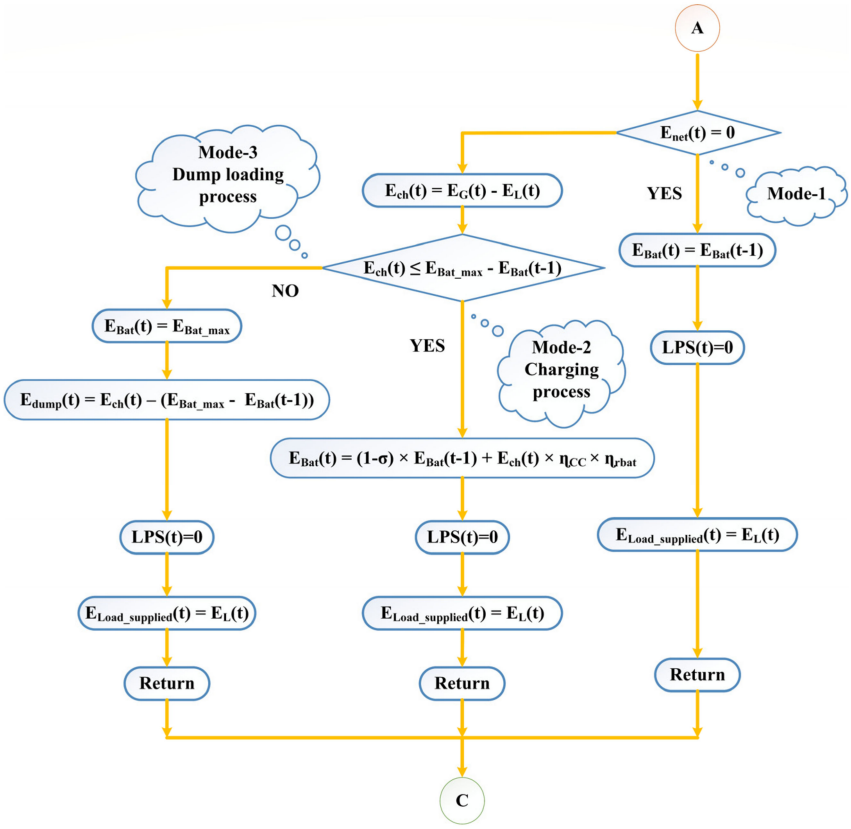

Figure 13. Flowchart of the EMS operating modes and acquisition of LPSP using LF and CC strategies.

7. Proposed Algorithm

The proposed algorithm of the study is a Salp Swarm Algorithm (SSA), which was identified in the literature from the metaheuristic family due to its proven ability to provide the global best optimal solutions to other recent scientific problems. Seyedali et al. [10] invented the SSA based on the salp swarm behavior. The salp is a small transparent organism and looks like a jellyfish with a barrel-shaped body as shown in Figure 14a. Salps also form a swarm like a chain in the deep ocean for searching and hunting for food, as shown in Figure 14b.

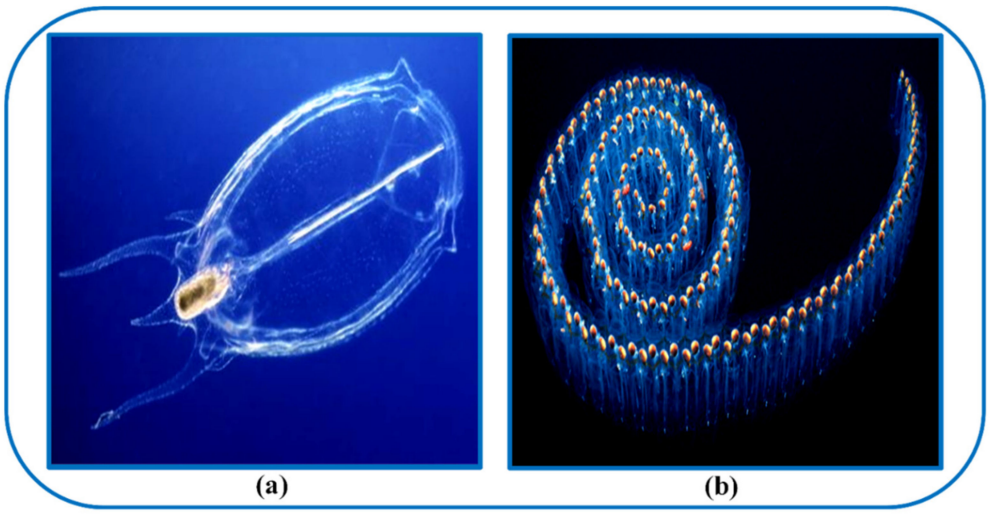

Figure 14. (**a**) Salp, (**b**) salp swarm chain.

Salp Swarm Algorithm (SSA)

The mathematical modelling of the salp chain population has been categorized into two groups such as a leader and followers. The leader salp stands in front of the chain and guides the remaining salps to follow behind it. Like other types of swarm-based optimization techniques, the location of the salps is stated in an n-dimensional search space, where n indicates the number of variables of the proposed objective. In this regard, the location of the salps was kept in a two-dimensional matrix of '*Z*', and it was presumed that food source '*f*' is presented in the search space as the swarm's goal.

To update the leader's position, Equation (80) is proposed.

$$Z_q^1 = \begin{cases} f_q + c_1 \times \left(\left(ul_q - ll_q \right) \times c_2 + ll_q \right), & c_3 \geq 0 \\ f_q - c_1 \times \left(\left(ul_q - ll_q \right) \times c_2 + ll_q \right), & c_3 < 0 \end{cases} \tag{80}$$

where Z_q^1 denotes the location of the leader salp in the qth dimension. ll_q and ul_q are the lower and upper limits of the qth dimension. c_1, c_2, and c_3 are the random numbers.

Equation (80) states that the leader itself can update its location as per the location of the food source. The most important parameter in balancing exploration and exploitation in SSA is the coefficient c_1, which is given in Equation (81).

$$c_1 = 2e^{-\left(\frac{4u}{U}\right)^2} \tag{81}$$

where u and U are the current and maximum number of iterations, respectively.

The random numbers c_2 and c_3 are generated uniformly in the interval of [0, 1]. These parameters direct the next location in the qth dimension and must be toward positive or negative infinity along with the step size. As per Newton's law of motion, the following equations are useful to update the location of the followers:

$$Z_q^i = \frac{1}{2} a t^2 + V_0 t \tag{82}$$

where, $i \geq 2$, Z_q^i represents the location of the ith follower salp in qth dimension, V_0 is the starting speed, t is time, and $a = \frac{V_{final}}{V_o}$. The time '$t$' is termed as an iteration and the difference between the two iterations is considered as one, and assuming $V_0 = 0$, then Z_q^i is calculated by using Equation (83).

$$Z_q^i = \frac{1}{2} \times \left(Z_q^i + Z_q^{i-1} \right) \tag{83}$$

where, $i \geq 2$, Z_q^i is the location of the ith follower salp in the qth dimension.

By using Equations (80) and (83), the salp chains are simulated.

The SSA solves optimization problems with its fast convergence property and obtains the global best optimal values quickly; furthermore, it has several advantages such as a simple concept, easy implementation, and high efficiency. The procedure followed to obtain the optimal sizing of the IHRES with SSA is explained clearly in the form of a flowchart shown in Figure 15.

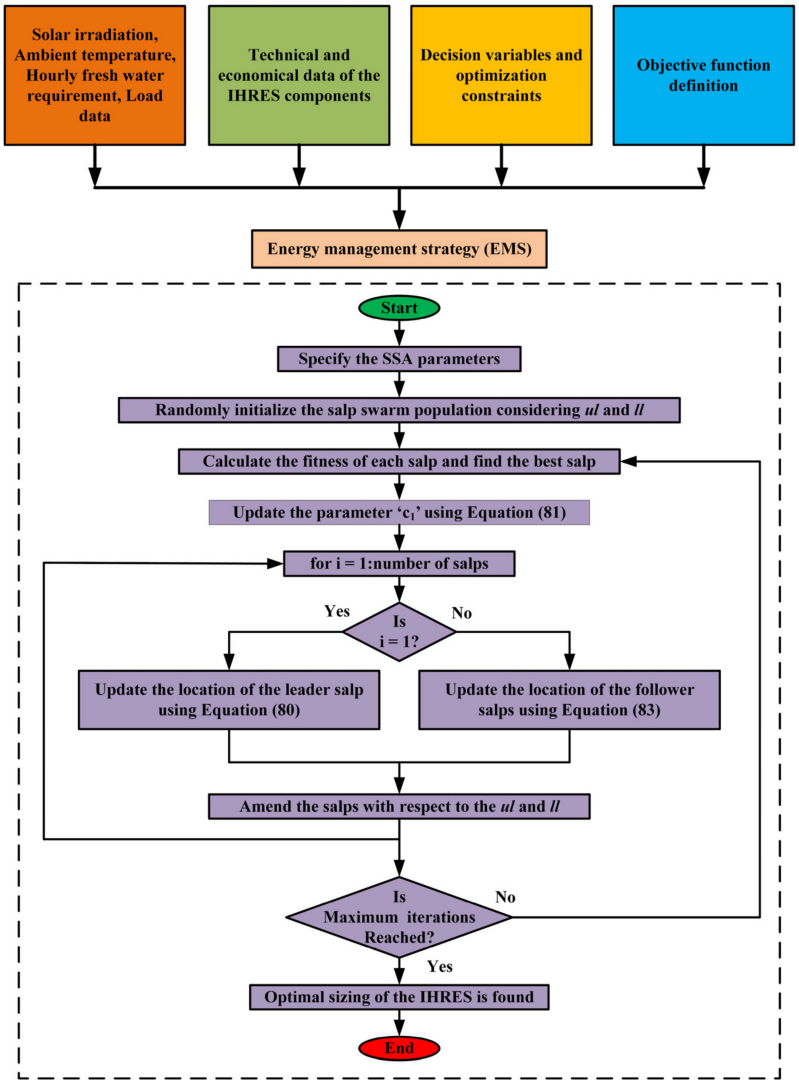

Figure 15. Flowchart illustrating the procedure for evaluating the optimal IRES sizing with SSA.

8. Results and Discussion

In this study, an optimal IHRES configuration was used to supply freshwater and electricity demands to five rural un-electrified villages in the Indian state of Odisha. These villages are enriched with RE resources such as biomass and solar, which can be used to electrify them. Because of the uncertainties associated with these RE sources, a reliable battery storage system in conjunction with a diesel generator is required to provide a continuous power supply. Therefore, the study focused on three different types of battery technologies, namely lithium-ion (Li-Ion), lead-acid (LA), and nickel-iron (Ni-Fe), to provide a continuous power supply.

The purpose of examining various battery technologies is the LA battery technology since it is less expensive in all regions of the world than all kinds of battery technologies. As a result, developing countries such as Pakistan, India, Sri Lanka, Bangladesh, etc., are employing this battery technology to electrify the standalone remote regions without taking into account significant drawbacks such as their durability and lifespan. This battery technology has a shorter lifespan in comparison to other battery technologies and its lifespan is dependent on the ambient temperature at which the batteries are installed. Therefore, every three to five years, they must be replaced. Frequently, replacing batteries in remote regions via difficult roads causes plenty of technical, physical, and economic issues. Hence, before beginning a project, it is indeed essential to understand the technological and economic features of a battery technology such as, technically: durability, high operating

temperature capability, longevity, and round trip efficiency, and economically: operation and maintenance costs, replacement frequency, and capital costs [43].

8.1. Robustness and History of the Ni-Fe Battery Technology

This study proposed a Ni-Fe battery technology to address the aforementioned issues. Although the Ni-Fe batteries are still in the early stages of development, they are the most powerful and reliable battery technology available today and are an excellent option for off-grid RE and solar applications. Ni-Fe batteries have a track record of more than 100 years. Thomas Edison invented and manufactured Ni-Fe batteries in the early 1900s to make them "much stronger than batteries using lead plates and acid". In the early 1910s, the first electric car was outfitted with Ni-Fe batteries. While they were never used for the starting batteries for internal combustion engines at the period of the automobile invention, their foothold was found in the twentieth century in many railroads, forklifts, and standby power applications. Because of their long life, robustness, and durability, Ni-Fe batteries have been reborn in the twenty-first century for use in RE applications.

In comparison to many other types of batteries, the depth of discharge (DOD) of the Ni-Fe batteries has no impact on their life cycle. As a result, consumers can discharge them up to 80% of their rated capacity and have a battery life of 30+ years. It is a well-known fact that if an LA battery is over-discharged even once, its lifetime is significantly reduced. This is true for the majority of battery technologies but not for the Ni-Fe batteries because discharging them up to 80% or more does not shorten their lifetime. Furthermore, Ni-Fe batteries can be overcharged without losing their life expectancy [50].

8.2. Technical Comparison of the Battery Technologies Used in the Study

The following are the technical characteristics of the three different types of battery technologies: Li-Ion, Ni-Fe, and LA.

8.2.1. The Lifetime of the Batteries

The battery's lifetime mainly depends on its depth of discharge (DOD); the DOD simply describes the degree to which the battery has been discharged in relation to its overall capacity. If the battery is fully discharged, then its DOD is 100%. According to the manufacturers, the three batteries, Ni-Fe, Li-Ion, and LA used in the study, have different lifespans depending on their use of the allowable DODs.

- The LA battery used in the study can be usable in two allowable DODs, such as 70% and 80%; if it is used at 70% DOD, its lifespan is 3 years; if it is used at 80% DOD, then its lifespan is 2.5 years.
- The Li-Ion battery used in the study can be usable in three allowable DODs, such as 50%, 70%, and 80%; if it is used at 50% DOD, its lifespan is 15 years; if it is used at 70% DOD, its lifespan is 9 years; if it is used at 80% DOD, its lifespan is 7.5 years.
- The Ni-Fe battery used in the study can be usable in two allowable DODs, such as 50% and 80%; if it is used at 50% DOD, its lifespan is 30+ years; if it is used at 80% DOD, its lifespan is also 30+ years. This is why it is the most robust battery technology because the DOD does not affect its lifespan and it is more suitable for off-grid rural electrification for people living in remote areas since it does not need to be replaced during the lifespan of the project.

8.2.2. Round Trip Efficiency of the Batteries

In view of the round trip efficiency of the batteries, the Li-Ion battery has the highest efficiency with 92%, the second best is the LA battery which has an efficiency of 85%, and the third best is the Ni-Fe battery which has an efficiency of 80%.

8.2.3. The Self-Discharge Rate of the Batteries

The Li-Ion battery has a self-discharge rate of 0.3%/day, the LA battery technology has a rate of 0.2%/day, and the Ni-Fe battery has a rate of 1%/day. However, in terms of

self-discharge energy losses, the Ni-Fe battery may have negligible losses. For example, if the Ni-Fe battery consumes 25 kWh of energy per day, the self-discharge energy loss is only 0.25 kWh, allowing the remaining 24.75 kWh to be used without any issue. Hence, the self-discharge losses with this battery technology are not that much higher.

8.2.4. Operating Temperature Capabilities of the Batteries

With the exception of the Ni-Fe battery technology, most batteries do not have high-temperature capabilities. The Ni-Fe battery offers worry-free service in extreme cold and hot conditions with working temperatures ranging from −30 °C to +60 °C. The second best is the Li-Ion battery technology with operating temperatures ranging from −20 °C to +50 °C. Finally, the third best is the LA battery technology with operating temperatures ranging from −20 °C to +45 °C.

8.2.5. Replacement Frequency of the Batteries during the Lifespan of the Project

The current study assumed a project life of twenty-five years, and if the LA battery was used in the study, it must be replaced 9 to 10 times at 70% and at 80% usage of DODs, respectively. If the study considered Li-Ion batteries, they would need to be replaced 2, 3, and 4 times, respectively, at 50%, at 70%, and at 80% usage of DODs. If the study considered the Ni-Fe battery, no replacement would be required during the lifespan of the project, either at 50% usage of DOD or at 80% usage of DOD, and it would operate for another five more years outside of the lifespan of the project.

8.2.6. Cycle Life of the Batteries

The number of charging and discharging cycles a battery can complete before losing its capacity is referred to as its cycle life. In this study, the LA battery technology has two-cycle lives, such as 800 and 750 cycles at 70% and at 80% DODs, respectively. The Li-Ion battery has three cycle lives, such as 5000, 3000, and 2500 cycles at 50%, at 70%, and at 80% DODs, respectively. The Ni-Fe battery has two cycle lives, such as 11,000+ and 11,000+ cycles at 50% and at 80% DODs, respectively. Compared to other battery technologies, the cycle life of the Ni-Fe battery technology is much higher.

8.3. Modelling of Different Configurations Using Battery Technologies and RE Resources

The Li-Ion battery can work at three different DODs, i.e., at 50%, at 70%, and at 80%; therefore, three configurations were modelled using the Li-Ion battery technology: PV/BMG/DG/Li-Ion at 50% DOD, PV/BMG/DG/Li-Ion at 70% DOD, and PV/BMG/DG/Li-Ion at 80% DOD. Similarly, the LA battery can work at two DODs such as at 70% and at 80%; therefore, two configurations were modelled using the LA battery technology: PV/BMG/DG/LA at 70% DOD and PV/BMG/DG/LA at 80% DOD. Similarly, the Ni-Fe battery can work at two different DODs, such as at 50% and at 80%; however, its primary strength is that it has a lifespan of more than 30 years at both the DODs. Hence, for the current study, the techno-economic analysis with Ni-Fe battery technology was accomplished with at 80% DOD only. As a result, a PV/BMG/DG/Ni-Fe at 80% DOD configuration was modelled.

In order to electrify the study area with an optimum configuration, the six configurations mentioned above were evaluated at an LPSP value of 0% with LF and CC strategies using the HPRALC-based scenario, i.e., without DSM. To simplify the analysis, after determining the optimal configuration from the HPRALC-based scenario, it was further evaluated with LF and CC strategies using MPRAMC and LPRAHC-based scenarios, i.e., with DSM at an LPSP value of 0%.

8.4. Optimization Algorithms and Components Technical and Cost Values

The proposed SSA algorithm's convergence efficiency and robustness were compared to those of eight other well-known and proven algorithms, namely: PSO, GA, GWO, DE, ALO, MFO, DA, and GOA in the MATLAB© environment with a population of 100 and 100 iterations. The nine algorithms' control parameter values are given in Table 4. All

components' cost and technical values used in the study are given in Tables 5–7. The peak load demand in the HPRALC-based scenario was 79.18 kW, hence the converter-rated power was 87 kW (for safety reasons, the converter's power rating should be 10% greater than the peak load demand). The peak load demand in the MPRAMC-based scenario was 54.44 kW. As a result, for the MPRAMC-based scenario, the converter-rated power was considered to be 60 kW. The peak load demand for the LPRAHC-based scenario was 52.02 kW. Hence, for MPRAMC-based scenarios, the converter-rated power was taken as 57 kW. Similarly, in order to meet the peak load demand of the HPRALC-based scenario, the DG-rated power was considered to be 80 kW, whereas in order to meet the peak load demand of the MPRAMC and LPRAHC-based scenarios, the DG-rated power was considered to be 60 kW because the commercially available rated power of the DG for these two scenarios is only 60 kW. Tables 8 and 9 give the optimal results of the six configurations described above with LF and CC strategies, respectively, using the nine metaheuristic algorithms at an LPSP value of 0% using the HPRALC-based scenario. The optimal configuration from the HPRALC-based scenario was further evaluated with LF and CC strategies at an LPSP value of 0% with MPRAMC and LPRAHC-based scenarios and their optimal results provided in Tables 10–13, respectively.

Table 4. Control parameters of the algorithms.

Algorithm	**Parameters**							
GA	Pop	$Iter_{max}$	μ	CR				
	100	100	0.1	0.9				
PSO	Pop	$Iter_{max}$	w_{max}	w_{min}	c1	c2		
	100	100	0.9	0.2	2	2		
DE	Pop	$Iter_{max}$	F	CR				
	100	100	0.5	0.9				
GWO	Pop	$Iter_{max}$	a	C1	C2	C3		
	100	100	0 to 2	2 × rand(0,1)	2 × rand(0,1)	2 × rand(0,1)		
ALO	Pop	$Iter_{max}$	I	weights				
	100	100	1	(1,5,3,15,8,1)				
DA	Pop	$Iter_{max}$	w	s	a	c	f	e
	100	100	0.9 to 0.2	0.1	0.1	0.7	1	1
MFO	Pop	$Iter_{max}$	a	b				
	100	100	−1 to −2	1				
GOA	Pop	$Iter_{max}$	c_{max}	c_{min}				
	100	100	1	0.00004				
SSA	Pop	$Iter_{max}$	c1	c2	c3			
	100	100	rand(0,1)	rand(0,1)	rand(0,1)			

Table 5. Batteries' techno-economic parameters and their values.

Battery Type	**Lead-Acid ($PbSO_4$)**	**Lithium Iron Phosphate ($LiFePO_4$)**	**Nickel-Iron (Ni-Fe)**
Manufacturer	Trojan [51]	Victron [52]	Iron Edison [50]
Model	SSIG 06 490	LFP-12.8/200-a	TN 1000
Nominal capacity (S_{BAT})	490 Ah	300 Ah	1000 Ah
Nominal voltage (V_{BAT})	6 V	12.8 V	1.2 V
Round trip efficiency (η_{rbat})	85%	92%	80%
Lifespan in years	3 years at 70% DOD	15 years at 50% DOD	30 years+ at 50% DOD
	2.5 years at 80% DOD	9 years at 70% DOD	30 years+ at 80% DOD
		7.5 years at 80% DOD	
Self-discharge rate (%/day) (σ)	0.3%	0.2%	1%
Capital cost (CC) in USD	USD 410	USD 3317	USD 1057
Annual O&M cost in USD	2.5% of CC	No maintenance	2% of CC
Operating temperature	−20°C to +45 °C	−20°C to +50 °C	−30 °C to +60 °C
Cycle life of the batteries	800 cycles at 70% DOD	5000 cycles at 50% DOD	11,000+ cycles at 50% DOD
	750 cycles at 80% DOD	3000 cycles at 70% DOD	11,000+ Cycles at 80% DOD
		2500 cycles at 80% DOD	

Table 6. Technical and cost values of the biomass generator.

Manufacturer [44]	**Enersol Bio Power**	**Water Tank Capacity [44]**	**300 L**
Rated Power of BMG [44]	5 kW	Frequency [44]	50 Hz
Fuel Mode [44]	100% Producer Gas Based	Life time of BMG [14]	15,000 h
Plant Size (L * W * H) [44]	10 * 9 * 6 Feet	BMG Capital cost [44]	USD 4505
Number of Phases [44]	Single Phase	AO&M cost of BMG [14]	USD 27
Rated Current [44]	26 Amperes	Quantity of biomass	9 t/year
Alternator Make [44]	Kirloskar Manufacturers	Cost of biomass [14]	15 USD/t
Voltage [44]	230 V, AC	Efficiency of BMG [14]	20%

Table 7. Technical and cost values of the IHRES.

Parameters	**Value**	**Parameters**	**Value**
Project lifetime	25 years	No. of MEM Repl./year [1]	2
Nominal interest rate [14]	13%	MEM Replacement cost [1]	0.06 USD/m^3
Inflation rate [53]	5%	Repl. cost of chemicals [1]	0.06 USD/m^3
Manufacturer of PV Panel [54]	Vikram solar	Rated power of converter for HPRALC scenario	87 kW
Model No. of PV Panel [54]	Somera 385	Rated power of converter for MPRAMC scenario	60 kW
Rated power of PV Panel [54]	385 Wp	Rated power of converter for LPRAHC scenario	57 kW
Lifetime of PV Panel [54]	25 years	Lifetime of converter [14]	10 years
Capital cost of PV Panel [54]	USD 128	C&R of converter per kW	USD 108
AO&M cost of PV Panel [14]	USD 3.2	AO&M cost of converter [14]	USD 15
Mechanical structure cost of PV Panel [55]	USD 41	Efficiency of converter [14]	95%

Table 7. *Cont.*

Parameters	Value	Parameters	Value
Life time of mechanical structure of PV panel [55]	25 years	DG (Company: Cummins, Model No: C100D5) for HPRALC scenario [56]	100 KVA 80 kW
ROD capital cost (1 m^3/day) [1]	USD 532	C&R of DG for HPRALC scenario [56]	USD 9144
Capital cost of Water tank [1]	256 USD/m^3	DG (Company: Kirloskar, Model No: KEC-T75-II) for MPRAMC and LPRAHC scenarios [57]	75 KVA 60 kW
Capital cost of membrane [1]	0.06 USD/m^3	C&R of DG for MPRAMC and LPRAHC scenarios [57]	USD 6858
Capital cost of chemicals [1]	0.06 USD/m^3	Diesel Price	USD 1.08
AO&M cost of ROD [1]	0.2 USD/m^3	AO&M cost of DG [46]	3% of TAOHDG"

Table 8. Optimization results of the HPRALC-based IHRESs using LF strategy at LPSP value of 0%.

Configuration	Q&C	GA	PSO	DE	GWO	ALO	DA	MFO	GOA	SSA
PV/	N_{PV}	1282	1280	1281	**1275**	1280	1280	1280	1280	**1275**
BMG/	N_{BAT}	917	917	879	**893**	917	917	917	917	**893**
DG/	AFC	1574	887	2192	**1600**	887	887	887	887	**1600**
Ni-Fe	ACO_2	4251	2395	5917	**4320**	2395	2395	2395	2395	**4320**
at DOD = 80%	LCC (USD)	918,176	918,040	921,542	**916,728**	918,040	918,040	918,040	918,040	**916,728**
PV/	N_{PV}	1243	**1237**	**1237**	1238	**1237**	**1237**	**1237**	**1237**	**1237**
BMG/	N_{BAT}	342	**340**	**340**	340	**340**	**340**	**340**	**340**	**340**
DG/	AFC	7338	**7499**	**7499**	7498	**7499**	**7499**	**7499**	**7499**	**7499**
LA	ACO_2	19,813	**20,247**	**20,247**	20,246	**20,247**	**20,247**	**20,247**	**20,247**	**20,247**
at DOD = 70%	LCC (USD)	1,516,213	**1,511,891**	**1,511,891**	1,512,129	**1,511,891**	**1,511,891**	**1,511,891**	**1,511,891**	**1,511,891**
PV/	N_{PV}	**1237**	**1237**	1301	**1237**	**1237**	**1237**	**1237**	**1237**	**1237**
BMG/	N_{BAT}	**297**	**297**	299	**297**	**297**	**297**	**297**	**297**	**297**
DG/	AFC	**7590**	**7590**	7123	**7590**	**7590**	**7590**	**7590**	**7590**	**7590**
LA	ACO_2	**20,494**	**20,494**	19,232	**20,494**	**20,494**	**20,494**	**20,494**	**20,494**	**20,494**
at DOD = 80%	LCC (USD)	**1,492,491**	**1,492,491**	1,506,249	**1,492,491**	**1,492,491**	**1,492,491**	**1,492,491**	**1,492,491**	**1,492,491**
PV/	N_{PV}	**1136**	**1136**	1183	1138	**1136**	**1136**	**1136**	**1136**	**1136**
BMG/	N_{BAT}	**339**	**339**	338	339	**339**	**339**	**339**	**339**	**339**
DG/	AFC	**7859**	**7859**	7895	7858	**7859**	**7859**	**7859**	**7859**	**7859**
Li-Ion	ACO_2	**21,220**	**21,220**	21,315	21,216	**21,220**	**21,220**	**21,220**	**21,220**	**21,220**
at DOD = 50%	LCC (USD)	**2,397,086**	**2,397,086**	2,403,931	2,397,563	**2,397,086**	**2,397,086**	**2,397,086**	**2,397,086**	**2,397,086**
PV/	N_{PV}	**1135**	**1135**	**1135**	**1135**	**1135**	1150	1211	**1135**	**1135**
BMG/	N_{BAT}	**242**	**242**	**242**	**242**	**242**	242	244	**242**	**242**
DG/	AFC	**7891**	**7891**	**7891**	**7891**	**7891**	7781	7172	**7891**	**7891**
Li-Ion	ACO_2	**21,307**	**21,307**	**21,307**	**21,307**	**21,307**	21,009	19,364	**21,307**	**21,307**
at DOD = 70%	LCC (USD)	**2,446,102**	**2,446,102**	**2,446,102**	**2,446,102**	**2,446,102**	2,447,773	2,467,615	**2,446,102**	**2,446,102**
PV/	N_{PV}	**1135**	**1135**	**1135**	**1135**	1203	1326	**1135**	1199	**1135**
BMG/	N_{BAT}	**212**	**212**	**212**	**212**	211	210	**212**	213	**212**
DG/	AFC	**7771**	**7771**	**7771**	**7771**	7837	7723	**7771**	7337	**7771**
Li-Ion	ACO_2	**20,981**	**20,981**	**20,981**	**20,981**	21,161	20,853	**20,981**	19,810	**20,981**
at DOD = 80%	LCC (USD)	**2,605,751**	**2,605,751**	**2,605,751**	**2,605,751**	2,611,090	2,624,535	**2,605,751**	2,621,122	**2,605,751**

Table 9. Optimization results of the HPRALC-based IHRES using CC strategy at LPSP value of 0%.

Configuration	Q&C	GA	PSO	DE	GWO	ALO	DA	MFO	GOA	SSA
PV/	N_{PV}	1268	**1265**	1332	1268	**1265**	**1265**	**1265**	**1265**	**1265**
BMG/	N_{BAT}	933	**928**	925	933	**928**	**928**	**928**	**928**	**928**
DG/	AFC	1045	**871**	821	1045	**871**	**871**	**871**	**871**	**871**
Ni-Fe	ACO_2	2822	**2352**	2217	2822	**2352**	**2352**	**2352**	**2352**	**2352**
at DOD = 80%	LCC (USD)	927,077	**926,800**	934,345	927,077	**926,800**	**926,800**	**926,800**	**926,800**	**926,800**
PV/	N_{PV}	**1178**	1202	**1178**	**1178**	**1178**	**1178**	1219	**1178**	**1178**
BMG/	N_{BAT}	**347**	394	**347**	**347**	**347**	**347**	346	**347**	**347**
DG/	AFC	**7839**	5823	**7839**	**7839**	**7839**	**7839**	7864	**7839**	**7839**
LA	ACO_2	**21,166**	15,723	**21,166**	**21,166**	**21,166**	**21,166**	21,233	**21,166**	**21,166**
at DOD = 70%	LCC (USD)	**1,525,952**	1,629,822	**1,525,952**	**1,525,952**	**1,525,952**	**1,525,952**	1,531,881	**1,525,952**	**1,525,952**
PV/	N_{PV}	**1174**	**1174**	1226	**1174**	**1174**	1213	**1174**	**1174**	**1174**
BMG/	N_{BAT}	**305**	**305**	306	**305**	**305**	304	**305**	**305**	**305**
DG/	AFC	**7640**	**7640**	7192	**7640**	**7640**	7615	**7640**	**7640**	**7640**
LA	ACO_2	**20,628**	**20,628**	19,419	**20,628**	**20,628**	20,561	**20,628**	**20,628**	**20,628**
at DOD = 80%	LCC (USD)	**1,503,917**	**1,503,917**	1,511,744	**1,503,917**	**1,503,917**	1,509,935	**1,503,917**	**1,503,917**	**1,503,917**
PV/	N_{PV}	**1098**	**1098**	1133	**1098**	**1098**	1082	**1098**	**1098**	**1098**
BMG/	N_{BAT}	**340**	**340**	340	**340**	**340**	341	**340**	**340**	**340**
DG/	AFC	**9083**	**9083**	9009	**9083**	**9083**	9059	**9083**	**9083**	**9083**
Li-Ion	ACO_2	**24,525**	**24,525**	24,324	**24,525**	**24,525**	24,458	**24,525**	**24,525**	**24,525**
at DOD = 50%	LCC (USD)	**2,416,367**	**2,416,367**	2,423,727	**2,416,367**	**2,416,367**	2,417,493	**2,416,367**	**2,416,367**	**2,416,367**
PV/	N_{PV}	**1084**	**1084**	**1084**	**1084**	1195	1930	1195	1225	**1084**
BMG/	N_{BAT}	**243**	**243**	**243**	**243**	241	235	241	241	**243**
DG/	AFC	**9083**	**9083**	**9083**	**9083**	9009	7366	9009	8735	**9083**
Li-Ion	ACO_2	**24,525**	**24,525**	**24,525**	**24,525**	24,324	19,889	24,324	23,585	**24,525**
at DOD = 70%	LCC (USD)	**2,463,960**	**2,463,960**	**2,463,960**	**2,463,960**	2,474,258	2,579,041	2,474,258	2,476,585	**2,463,960**
PV/	N_{PV}	1177	**1116**	**1116**	1176	1486	1516	**1116**	1176	**1116**
BMG/	N_{BAT}	211	**212**	**212**	211	208	208	**212**	211	**212**
DG/	AFC	9083	**9108**	**9108**	9083	8138	7964	**9108**	9083	**9108**
Li-Ion	ACO_2	24,525	**24,593**	**24,593**	24,525	21,972	21,502	**24,593**	24,525	**24,593**
at DOD = 80%	LCC (USD)	2,629,251	**2,627,111**	**2,627,111**	2,629,041	2,645,568	2,648,554	**2,627,111**	2,629,041	**2,627,111**

Table 10. Optimization results of the MPRAMC-based IHRES using LF strategy at LPSP value of 0%.

Configuration	Q&C	GA	PSO	DE	GWO	ALO	DA	MFO	GOA	SSA
PV/	N_{PV}	**904**	**904**	921	**904**	**904**	**904**	**904**	**904**	**904**
BMG/	N_{BAT}	**569**	**569**	563	**569**	**569**	**569**	**569**	**569**	**569**
DG/	AFC	**854**	**854**	1010	**854**	**854**	**854**	**854**	**854**	**854**
Ni-Fe	ACO_2	**2306**	**2306**	2726	**2306**	**2306**	**2306**	**2306**	**2306**	**2306**
at DOD = 80%	LCC (USD)	**613,841**	**613,841**	617,660	**613,841**	**613,841**	**613,841**	**613,841**	**613,841**	**613,841**

Table 11. Optimization results of the MPRAMC-based IHRES using CC strategy at LPSP value of 0%.

Configuration	Q&C	GA	PSO	DE	GWO	ALO	DA	MFO	GOA	SSA
PV/	N_{PV}	877	**890**	903	891	**890**	877	**890**	877	**890**
BMG/	N_{BAT}	594	**599**	588	596	**599**	594	**599**	594	**599**
DG/	AFC	989	**653**	915	747	**653**	989	**653**	989	**653**
Ni-Fe	ACO_2	2671	**1764**	2469	2016	**1764**	2671	**1764**	2671	**1764**
at DOD = 80%	LCC (USD)	623,772	**623,484**	625,477	623,808	**623,484**	623,772	**623,484**	623,772	**623,484**

Table 12. Optimization results of the LPRAHC-based IHRES using LF strategy at LPSP value of 0%.

Configuration	Q&C	GA	PSO	DE	GWO	ALO	DA	MFO	GOA	SSA
PV/	N_{PV}	**814**	**814**	834	**814**	**814**	**814**	**814**	**814**	**814**
BMG/	N_{BAT}	**450**	**450**	458	**450**	**450**	**450**	**450**	**450**	**450**
DG/	AFC	**837**	**837**	532	**837**	**837**	**837**	**837**	**837**	**837**
Ni-Fe	ACO_2	**2259**	**2259**	1438	**2259**	**2259**	**2259**	**2259**	**2259**	**2259**
at DOD = 80%	LCC (USD)	**522,945**	**522,945**	526,708	**522,945**	**522,945**	**522,945**	**522,945**	**522,945**	**522,945**

Table 13. Optimization results of the LPRAHC-based IHRES using CC strategy at LPSP value of 0%.

Configuration	Q&C	GA	PSO	DE	GWO	ALO	DA	MFO	GOA	SSA
PV/	N_{PV}	**791**	**791**	794	**791**	**791**	**791**	801	**791**	**791**
BMG/	N_{BAT}	**496**	**496**	495	**496**	**496**	**496**	487	**496**	**496**
DG/	AFC	**131**	**131**	149	**131**	**131**	**131**	280	**131**	**131**
Ni-Fe	ACO_2	**353**	**353**	403	**353**	**353**	**353**	756	**353**	**353**
at DOD = 80%	LCC (USD)	**529,795**	**529,795**	530,336	**529,795**	**529,795**	**529,795**	530,042	**529,795**	**529,795**

8.5. Optimal Configuration from the LA Battery-Based IHRESs

The LA battery can operate at two different DODs, i.e., at 70% and at 80%. In such a way that a total of two configurations were modelled using LA battery technology and which were tested with two different dispatch strategies such as LF and CC, their corresponding results using the HPRALC-based scenario are provided in Tables 8 and 9, respectively. From the results, it was observed that the LA battery-based IHRES at 80% DOD with LF strategy is economically feasible as compared to its CC strategy, as well as LA battery-based IHRES at 70% DOD using LF and CC strategies, with an LCC of USD 1,492,491. It is about 1% lower than its CC strategy's LCC, and it is about 1% and 2% lower than the LCCs of LA battery-based IHRES at 70% DOD using LF and CC strategies, respectively. The corresponding optimum component values were N_{PV} = 1237 and $N_{BAT\ (LA)}$ = 297. Therefore, for further comparisons with other battery-based IHRESs, the LA battery-based IHRES at 80% DOD with LF strategy was taken into account.

The Effect of Dispatch Strategies on LA Battery-Based IHRESs

The above discussion reveals that the LA battery-based IHRES at 80% DOD with LF strategy was identified as an optimal configuration; its annual fuel consumption (AFC) and annual carbon dioxide (ACO_2) emissions compared to other dispatch strategies (LF and CC) of the remaining LA battery-based IHRESs are discussed as follows:

From the results given in Tables 8 and 9, it is observed that the AFC of the LA battery-based IHRES at 80% DOD with LF strategy was 7590 L, which is 50 L less than its CC strategy's AFC, as well as 91 L more and 249 L less than the LA battery-based IHRES at 70% DOD's LF and CC strategies' AFCs, respectively.

From the results given in Tables 8 and 9, it is observed that the ACO_2 emissions of the LA battery-based IHRES at 80% DOD with LF strategy was 20,494 kg, which is 134 kg less than the ACO_2 emissions of its CC strategy, as well as 316 and 247 kg more and 672 kg less than the ACO_2 emissions of the LA battery-based IHRES at 70% DOD's LF and CC strategies, respectively.

8.6. Optimal Configuration from the Li-Ion Battery-Based IHRESs

The Li-Ion battery can operate at three different DODs, i.e., at 50%, at 70%, and at 80%. In such a way that a total of three configurations were modelled using Li-Ion battery technology and which were tested with two dispatch strategies such as LF and CC, their corresponding

optimal results using the HPRALC-based scenario are provided in Tables 8 and 9, respectively. From the results, it was observed that the Li-Ion battery-based IHRES at 50% DOD with LF strategy is economically feasible as compared to its CC strategy, as well as Li-Ion battery-based IHRESs at 70% and at 80% DOD's LF and CC strategies, with an LCC of USD 2,397,086. It is about 1% lower than its CC strategy's LCC, and it is about 2%, 3%, 8%, and 9% lower than the LCCs of Li-Ion battery-based IHRESs at 70% and at 80% DOD's LF and CC strategies. The corresponding optimum component values of N_{PV} and $N_{BAT\ (Li\text{-}Ion)}$ were 1136 and 339, respectively. Therefore, for further comparisons with other battery-based IHRESs, the Li-Ion battery-based IHRES at 50% DOD with LF strategy was taken into account.

The Effect of Dispatch Strategies on Li-Ion Battery-Based IHRESs

The above discussion reveals that the Li-Ion battery-based IHRES at 50% DOD with LF strategy was identified as an optimal configuration; its AFC and ACO_2 emissions compared to other dispatch strategies (LF and CC) of the remaining Li-Ion battery-based IHRESs are discussed as follows:

From the results given in Tables 8 and 9, it is observed that the AFC of the Li-Ion battery-based IHRES at 50% DOD with LF strategy was 7859 L, which is 1224 L less than its CC strategy's AFC and 32 and 1224 L less than the Li-Ion battery-based IHRES at 70% DOD's LF and CC strategies' AFCs, respectively, as well as 88 L more and 1249 L less than the Li-Ion battery-based IHRES at 80% DOD's LF and CC strategies' AFCs, respectively.

From the results given in Tables 8 and 9, it is observed that the ACO_2 emissions of the Li-Ion battery-based IHRES at 50% DOD with LF strategy was 21,220 kg, which is 3305 kg less than its CC strategy's ACO_2 emissions and 87 kg and 3305 kg less than the Li-Ion battery-based IHRES at 70% DOD's LF and CC strategies' ACO_2 emissions, respectively, as well as 239 kg more and 3373 kg less than the Li-Ion battery-based IHRES at 80% DOD's LF and CC strategies' ACO_2 emissions, respectively.

8.7. Optimal Configuration from the Ni-Fe Battery-Based IHRESs

The Ni-Fe battery can operate at two different DODs, such as at 50% and at 80%, and it has a lifespan of more than 30+ years at both the DODs. Therefore, the analysis was conducted at 80% DOD only with two different dispatch strategies such as LF and CC, and its corresponding optimal results using the HPRALC-based scenario are provided in Tables 8 and 9, respectively. From the results, it is observed that the Ni-Fe battery-based IHRES at 80% DOD with LF strategy was identified as an optimal configuration as compared to its CC strategy, with an LCC of USD 916,728. It is about 1% lower than its CC strategy's LCC. The corresponding optimum component values were N_{PV} = 1275 and $N_{BAT\ (Ni\text{-}Fe)}$ = 893. Therefore, for further comparisons with other battery-based IHRESs, the Ni-Fe battery-based IHRES at 80% DOD with LF strategy was considered.

The Effect of Dispatch Strategies on Ni-Fe Battery-Based IHRESs

The above discussion reveals that the Ni-Fe battery-based IHRES at 80% DOD with CC strategy was identified as an optimal configuration; its AFC and ACO_2 emissions compared to its LF strategy are discussed as follows:

From the results given in Tables 8 and 9, it is observed that the AFC of the Ni-Fe battery-based IHRES at 80% DOD with LF strategy was 1600 L, which is 729 L more than its CC strategy's AFC.

From the results given in Tables 8 and 9, it is observed that the ACO_2 emission of the Ni-Fe battery-based IHRES at 80% DOD with LF strategy was 4320 kg, which is 1968 kg more than its CC strategy's ACO_2 emissions.

8.8. The System Performance with Different Battery Technologies Using HPRALC, MPRAMC, and LPRAHC-Based Scenarios

The following describes the impact of different battery technologies and dispatch strategies on evaluating an optimal configuration using three efficiency-based scenarios: HPRALC, MPRAMC, and LPRAHC.

8.8.1. Low-Efficiency Appliance Usage-Based Scenario (HPRALC) (without DSM)

A low-efficiency appliance usage-based scenario refers to the usage of high power rated appliances of low cost (HPRALC) by the consumers, which falls under the concept without DSM. According to the results given in Tables 8 and 9 for the HPRALC-based scenario, it is observed that the Ni-Fe battery-based IHRES at 80% DOD with LF strategy (base case) provided an LCC of USD 916,728. It is an optimal value when compared to other battery-based IHRES LCCs with different dispatch strategies. The LA battery-based IHRES at 80% DOD with LF strategy provided an optimal LCC of USD 1,492,491, which is about 63% higher than the base case LCC. The Li-Ion battery-based IHRES at 50% DOD with LF strategy provided an optimal LCC of USD 2,397,086, which is about 162% higher than the base case LCC.

The Effect of Dispatch Strategies with Different Battery Technologies Using Low-Efficiency Appliance Usage-Based Scenario (HPRALC) (without DSM)

From the results given in Tables 8 and 9, it is observed that the AFC of the Ni-Fe battery-based IHRES at 80% DOD with LF strategy was 1600 L, which is 5990 L less than the AFC of LA battery-based IHRES at 80% DOD's LF strategy, and it is 6259 L less than the AFC of Li-Ion battery-based IHRES at 50% DOD's LF strategy.

From the results given in Tables 8 and 9, it is observed that the ACO_2 emission of the Ni-Fe battery-based IHRES at 80% DOD with LF strategy was 4320 kg, which is 16,174 kg less than the ACO_2 emissions of LA battery-based IHRES at 80% DOD's LF strategy, and it is 16,900 kg less than the ACO_2 emission of the Li-Ion battery-based IHRES at 50% DOD's LF strategy.

Finally, it was found that the Ni-Fe battery-based IHRES with LF strategy is more suitable for electrifying the study area. It is clear from the preceding Section 8.8.1 that Ni-Fe battery-based IHRES with LF strategy is more economically feasible as compared to its CC strategy and other battery-based IHRESs with different dispatch strategies, and it is also more eco-friendly in terms of annual fuel consumption and carbon emissions due to its lower fuel consumption and carbon emissions as compared to other battery-based IHRESs with different dispatch strategies. Therefore, IHRESs based on LA and Li-Ion batteries are not considered for further analysis in Section 8.8.2 (MPRAMC-based scenario) and Section 8.8.3 (LPRAHC-based scenario), since it is clear from the above discussion that these two battery technologies are not economically and environmentally feasible when compared to the Ni-Fe battery technology.

8.8.2. The Effect of Ni-Fe Battery-Based IHRES Using Medium-Efficiency Appliance Usage-Based Scenario (MPRAMC) (with DSM)

From the results of the low-efficiency appliance usage-based scenario (HPRALC), it was identified that the Ni-Fe battery-based IHRES with LF strategy (base case) provided a minimum LCC when compared to its CC strategy, as well as other battery-based IHRESs with different dispatch strategies. Therefore, this configuration was further analyzed with the medium-efficiency appliance usage-based scenario, i.e., with DSM. The medium-efficiency appliance usage-based scenario refers to the usage of medium power rated appliances of moderate cost (MPRAMC) by the consumers and it is a part of the concept of energy conservation-based DSM. From the results given in Tables 10 and 11, it is observed that the base case LCC with the MPRAMC-based scenario with LF strategy was USD 613,841, which is about 2% lower than its CC strategy's LCC, as well as about 33% lower than the LCC using the HPRALC-based scenario with LF strategy. The current scenario optimum component values are N_{PV} = 904 and $N_{BAT\ (Ni\text{-}Fe)}$ = 569. If these values were

compared to the HPRALC-based scenario values, it was observed that the required number of PV panels was reduced from 1275 to 904, i.e., a reduction in requirement of 371 PV panels, and the required number of batteries was reduced from 893 to 569, i.e., a reduction in requirement of 324 batteries.

The Effect of Different Dispatch Strategies on the Ni-Fe Battery-Based IHRES Using Medium-Efficiency Appliance Usage-Based Scenario (MPRAMC) (with DSM)

From the results given in Tables 10 and 11, it is observed that the AFC of the Ni-Fe battery-based IHRES at 80% DOD with LF strategy using the medium-efficiency appliance usage-based scenario was 854 L, which is 201 L more than the AFC using the CC strategy, as well as 746 L less than the AFC using the HPRALC-based scenario's LF strategy.

From the results given in Tables 10 and 11, it is observed that the ACO_2 emission of the Ni-Fe battery-based IHRES at 80% DOD with LF strategy using the medium-efficiency appliance usage-based scenario was 2306 kg, which is 542 kg more than the ACO_2 emission using the CC strategy, as well as 2014 kg less than the ACO_2 emission using the HPRALC-based scenario's LF strategy.

Therefore, it was concluded that the usage of medium power rated appliances of moderate cost has a significant effect on the system performance due to the reduction of both the LCC and the required number of components.

8.8.3. The Effect of Ni-Fe Battery-Based IHRES Using High-Efficiency Appliance Usage-Based Scenario (LPRAHC) (with DSM)

From the results of the low-efficiency appliance usage-based scenario (HPRALC), the Ni-Fe battery-based IHRES with LF strategy (base case) provided the lowest LCC when compared to its CC strategy and other battery-based IHRESs with different dispatch strategies. Therefore, this configuration was further analyzed with a high-efficiency appliance usage-based scenario, i.e., with DSM. The high-efficiency appliance usage-based scenario means the usage of low power rated appliances of high cost (LPRAHC) by the consumers and is a part of the concept of the energy conservation-based DSM. The results given in Tables 12 and 13 showed that the base case with LF strategy provided an LCC with the LPRAHC-based scenario of USD 522,945, which is about 1% lower than its CC strategy's LCC, as well as about 43% and 15% lower than its LCCs with the LF strategy using the HPRALC and MPRAMC-based scenarios, respectively. The current scenario's optimal component values were N_{PV} = 814 and $N_{BAT\ (Ni\text{-}Fe)}$ = 450. If these values were compared to the HPRALC-based scenario values, the number of PV panels was reduced from 1275 to 814, i.e., a reduction in the requirement of 461 PV panels, and the number of batteries was reduced from 893 to 450, i.e., a reduction in the requirement of 443 batteries. Similarly, if these values were compared to the MPRAMC-based scenario values, the required number of PV panels was reduced from 904 to 814, i.e., a reduction in the requirement of 90 PV panels, and the number of batteries was reduced from 569 to 450, i.e., a reduction in the requirement of 119 batteries.

The Effect of Different Dispatch Strategies on the Ni-Fe Battery-Based IHRES Using High-Efficiency Appliance Usage-Based Scenario (LPRAHC) (with DSM)

From the results given in Tables 12 and 13, it is observed that the AFC of the Ni-Fe battery-based IHRES at 80% DOD with LF strategy using the high-efficiency appliance usage-based scenario was 837 L, which is 706 L more than its AFC using the CC strategy and 763 L less than its AFC using the HPRALC-based scenario's LF strategy, as well as 17 L less than its AFC using the MPRAMC-based scenario's LF strategy.

According to the results given in Tables 12 and 13, it is observed that the ACO_2 emission of the Ni-Fe battery-based IHRES at 80% DOD with LF strategy using the high-efficiency appliance usage-based scenario was 2259 kg, which is 1906 kg more than its ACO_2 emission using the CC strategy and 2061 kg less than its ACO_2 emission using the HPRALC-based scenario's LF strategy, as well as 47 kg less than its ACO_2 emission using MPRAMC-based scenario's LF strategy.

Therefore, it was observed that the usage of low power rated appliances of high cost has moderate and significant effects on the system performance due to a reduction in both the LCC and the required number of components when compared to medium and low-efficiency appliance usage-based scenarios' optimal values. Finally, it was concluded that the Ni-Fe battery-based IHRES with LF strategy using the high-efficiency appliance usage-based scenario (LPRAHC) is best suited to electrify the study area while comparing to other battery-based IHRESs as well as other efficiency-based scenarios. Furthermore, because of India's well-known energy-efficient appliance usage schemes as stated in the introduction, electrification based on the LPRAHC-based scenario is more cost-effective for both the consumers and the government. Particularly in view of the electricity bills, this LPRAHC-based scenario electrification is more beneficial for people living in off-grid rural areas.

Figures 16 and 17 show the energy graphs of the different components for one week in both the summer and winter seasons, respectively, for the Ni-Fe battery-based IHRES with CC strategy using the LPRAHC-based scenario, According to the figures, the PV panels only supply the load demand from morning to evening (8 A.M. to 4 P.M. in winter and from 7 A.M. to 5 P.M. in summer). During this period, it is advantageous to charge the battery bank with excess energy generated by the PV panels.

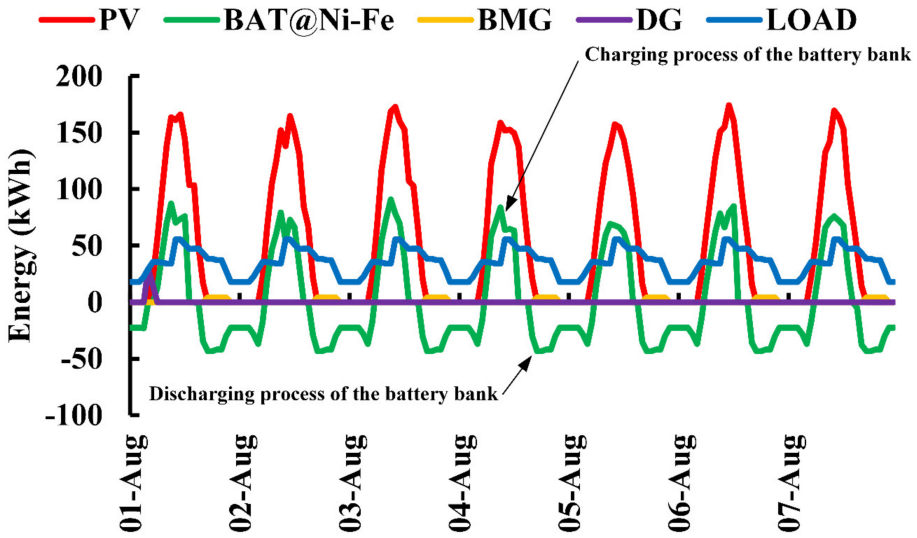

Figure 16. During one week of the summer season in August, energy outputs of various components of the Ni-Fe battery-based IHRES with LF strategy using LPRAHC loads.

PV panels cannot produce energy from the evening. Therefore, the batteries supply the deficit load demand through the discharge mechanism in order to provide a continuous power supply that meets the greatest amount of load demand. In addition, the biomass generator operates in conjunction with the battery bank discharge mechanism to satisfy the peak load demands from 6 P.M. to 10 P.M. and contributes to the marginal peak load demands. The total load demand is supplied exclusively by the batteries after 10 P.M. until the morning hours of 7 A.M. to 8 A.M., and this cyclic process is repeated for all days of the winter and summer seasons. Furthermore, as seen in the summer season energy graph, the DG comes into operation during certain peak hours of the summer season when batteries are unable to meet the peak load demands.

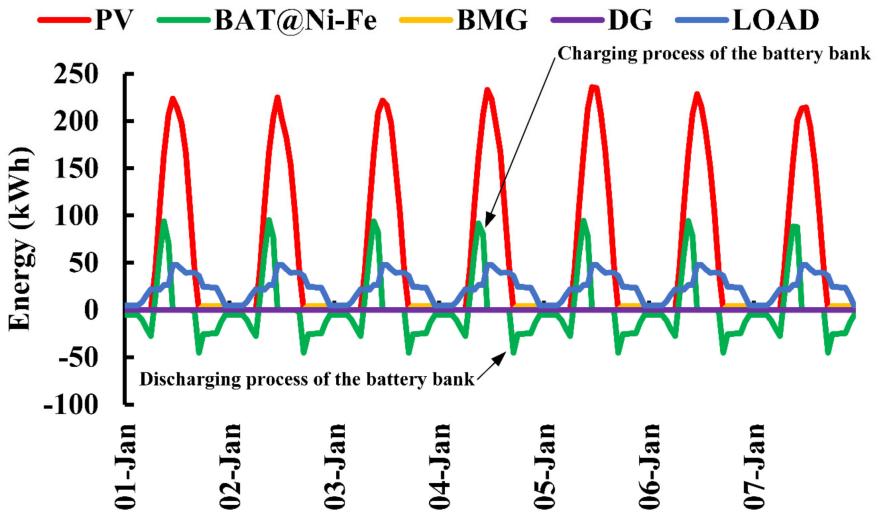

Figure 17. During one week of the winter season in January, energy outputs of various components of the Ni-Fe battery-based IHRES with LF strategy using LPRAHC loads.

8.9. Robustness of the Algorithms in Finding the Global Best Optimal Values

From the results provided for the three scenarios of sixteen configurations from Tables 8–13, the robustness of the algorithms can be analyzed. Among these sixteen configurations, the DE algorithm provided the global best optimal values for only six configurations and obtained the 6th rank in providing the global best optimal values. The DA algorithm provided the global best optimum values for eight configurations and obtained the 5th rank. The GA, GWO, MFO, and GOA algorithms provided the global best optimum values for eleven configurations and obtained the 4th rank. The ALO algorithm provided the global best optimum values for twelve configurations and obtained the 3rd rank. The PSO algorithm provided the global best optimum values for fourteen configurations and obtained the 2nd rank. Finally, the SSA algorithm provided the global best optimum values for all sixteen configurations and obtained the 1st rank in finding the global best optimum values and proven its robustness when compared to other algorithms.

8.10. Convergence Efficiency of the Algorithms in Finding the Global Best Optimal Values

Each optimized value obtained in each iteration of the simulation process of each algorithm was used to draw the convergence curves, which are shown from Figures 18–22. We used a total of 100 iterations for the current study. The marble symbol in the figures below indicates that the algorithm reached its global best optimal value on that number of iteration. If an algorithm does not have a marble symbol, it does not have the global best optimal value. Figure 18 shows the convergence curves of all algorithms for the Ni-Fe battery-based IHRES at 80% DOD with LF strategy using the HPRALC-based scenario; these curves are useful to evaluate the convergence efficiency of the algorithm with respect to other algorithms in finding the global best optimal values. This configuration obtained the minimum LCC with GWO and **SSA** algorithms at the 98th and 27th iteration, respectively.

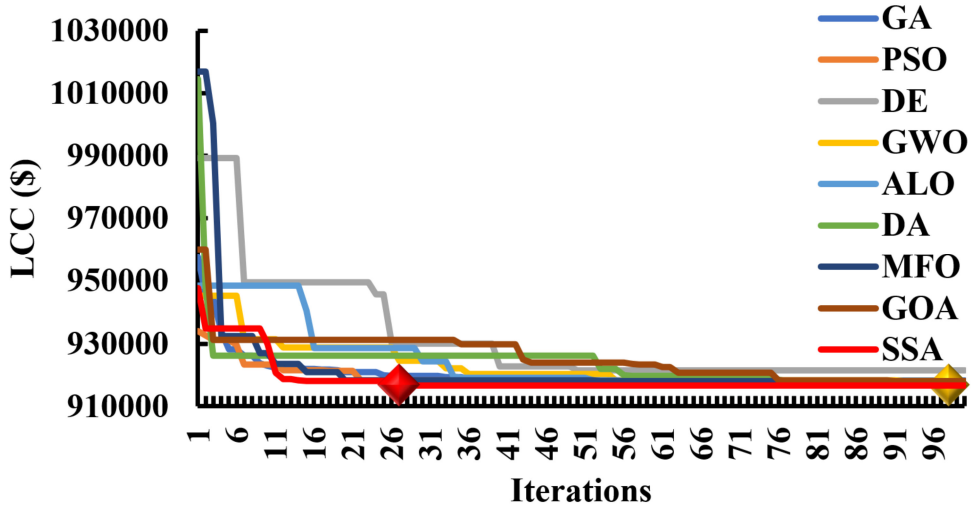

Figure 18. Convergence curves of the Ni-Fe battery-based IHRES with LF strategy using HPRALC-based scenario.

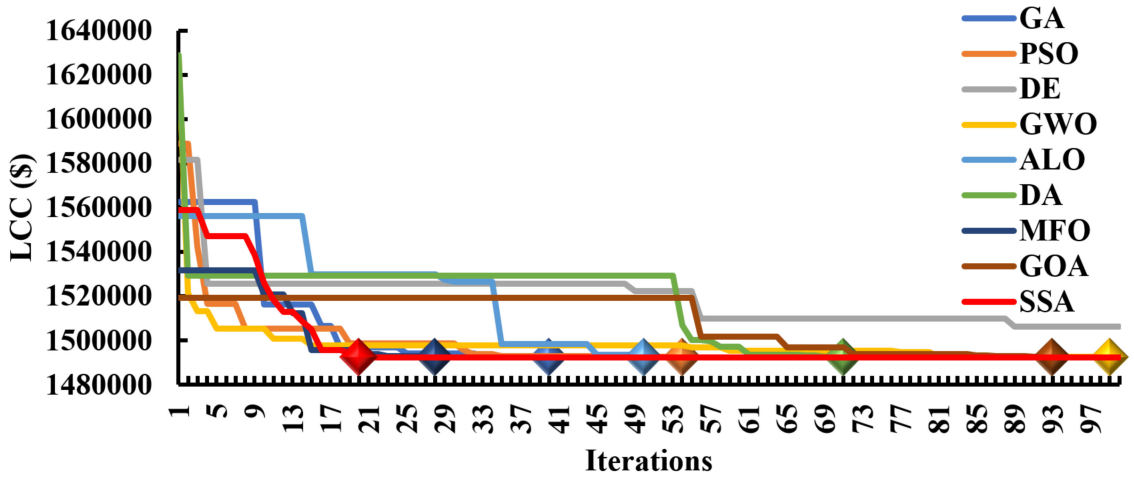

Figure 19. Convergence curves of LA at 80% DOD with HPRALC.

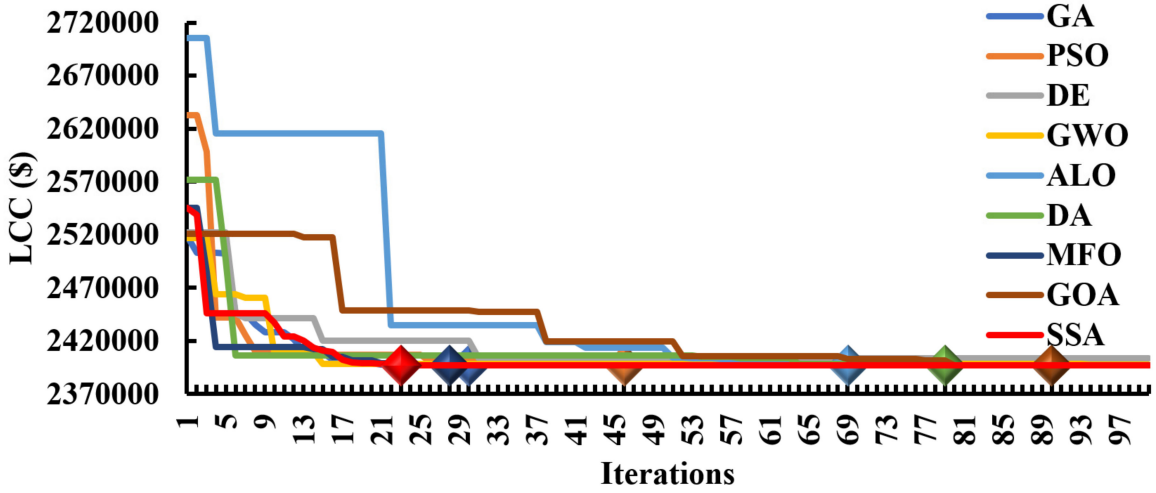

Figure 20. Convergence curves of Li-Ion at 50% DOD with HPRALC.

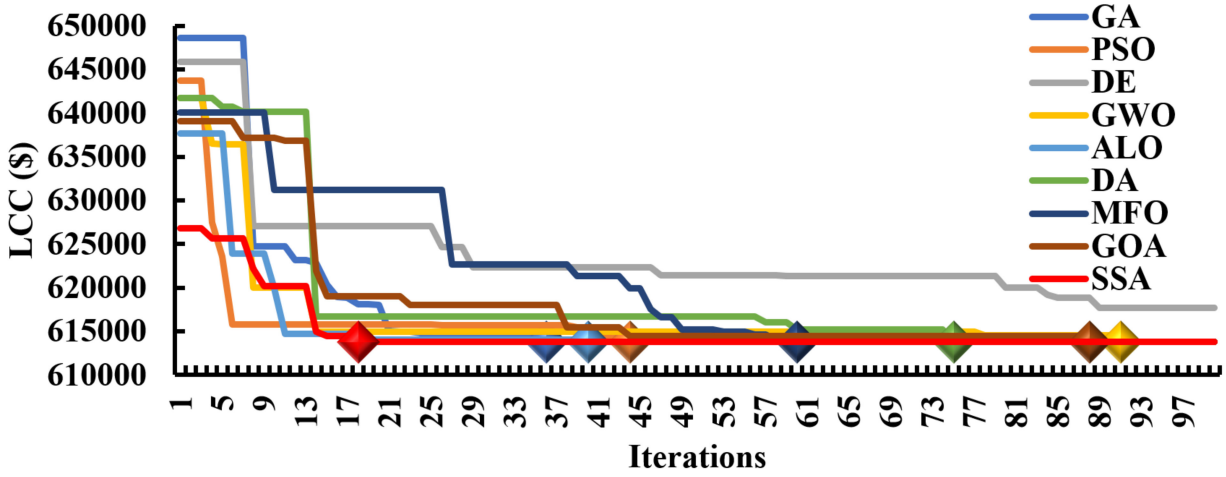

Figure 21. Convergence curves of Ni-Fe based IHRES with MPRAMC.

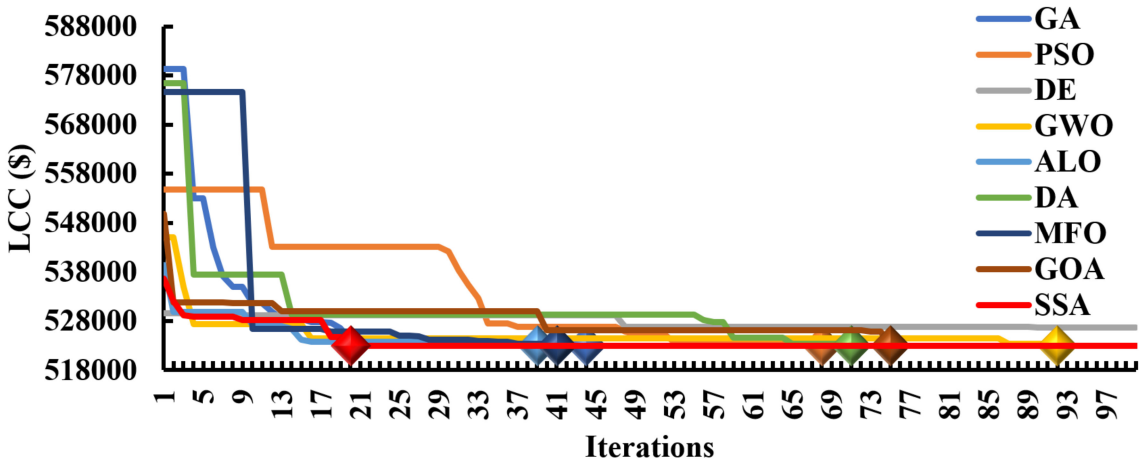

Figure 22. Convergence curves of Ni-Fe based IHRES with LPRAHC.

Figure 19 shows the convergence curves of all algorithms for the LA battery-based IHRES at 80% DOD with LF strategy using the HPRALC-based scenario. This configuration obtained the minimum LCC with GA, PSO, GWO, ALO, DA, MFO, GOA, and **SSA** algorithms at the 40th, 54th, 99th, 50th, 71st, 28th, 93rd, and **20th** iteration, respectively.

Figure 20 shows the convergence curves of all algorithms for the Li-Ion battery-based IHRES at 50% DOD with LF strategy using the HPRALC-based scenario. This configuration obtained the minimum LCC with GA, PSO, ALO, DA, MFO, GOA, and **SSA** algorithms at the 30th, 46th, 69th, 79th, 28th, 90th, and **23rd** iteration, respectively.

Figure 21 shows the convergence curves of all algorithms for the Ni-Fe battery-based IHRES at 80% DOD with LF strategy using the MPRAMC-based scenario. This configuration obtained a minimum LCC with GA, PSO, GWO, ALO, DA, MFO, GOA, and **SSA** algorithms at the 36th, 44th, 91st, 40th, 75th, 60th, 88th, and **18th** iteration, respectively.

Figure 22 shows the convergence curves of the Ni-Fe battery-based IHRES at 80% DOD with LF strategy using the LPRAHC-based scenario, the minimum LCC of this configuration obtained with GA, PSO, DE, GWO, ALO, DA, MFO, GOA, and **SSA** algorithms at the 44th, 68th, 92nd, 39th, 71st, 41st, 75th, and **20th** iteration, respectively.

From Sections 8.9 and 8.10, it was noted that in all sixteen configurations with different scenarios, the proposed SSA algorithm showed its robustness and convergence efficiency in finding the global best optimal values. Therefore, the proposed SSA algorithm is strongly recommended for microgrid size issues.

9. Sensitivity Analysis

To determine the LCC variability of the optimal configuration, i.e., Ni-Fe battery-based IHRES at 80% DOD with LF strategy using the LPRAHC-based scenario, a sensitivity analysis with a ±20% variance in input parameters such as biomass collection rate, interest rate, and diesel prices was performed as follows:

The optimum configuration was referred to as a base case and its achieved LCC was USD 522,945, with input parameters such as interest rate, biomass collection rate, and diesel prices being 60%, 13%, and 1.08 USD/L, respectively.

Table 14 shows that increasing the system interest rate by 10% to 20% of its base rate raised the system LCC from 4.47% to 9.95% in comparison to the base case LCC. Similarly, if the system's interest rate was reduced from 10% to 20%, the system's LCC could be reduced from 3.68% to 6.73% in comparison to its base case LCC, and it was concluded that the interest rate has a significant effect on the system performance.

Table 14. Optimal configuration results with interest rate variation.

Growth	−20% of Base Case	−10% of Base Case	Base Case	+10% of Base Case	+20% of Base Case
Interest Rate	10.4%	11.7%	**13%**	14.3%	15.6%
LCC (USD)	487,769	503,712	**522,945**	546,335	574,958

Table 15 shows that raising the biomass collection rate by 10% to 20% of its base rate reduced the system LCC from 0.31% to 0.67% compared to the base case LCC. Similarly, lowering the system's biomass collection rate from 10% to 20% increased the system's LCC from 0.35% to 0.68% in relation to the base case LCC, and it was concluded that the biomass collection rate has a negligible effect on the system performance.

Table 15. Optimal configuration results with the variation of biomass collection rate.

Growth	−20% of Base Case	−10% of Base Case	Base Case	+10% of Base Case	+20% of Base Case
Biomass collection rate	48%	54%	**60%**	66%	72%
Available tons of biomass	7.2	8.1	**9**	9.9	10.8
LCC (USD)	526,524	524,753	**522,945**	521,316	519,443

Table 16 shows that increasing the diesel prices by 10% to 20% of its base rate raised the system LCC from 0.3% to 0.61% in comparison to the base case LCC. Similarly, if the system's interest rate was reduced from 10% to 20%, the system's LCC could be reduced from 0.51% to 0.61% in comparison to its base case LCC, and it was concluded that the diesel prices have a negligible effect on the system performance.

Table 16. Optimal configuration results with the variation of diesel price.

Growth	−20% of Base Case	−10% of Base Case	Base Case	+10% of Base Case	+20% of Base Case
Diesel price/L (USD)	0.864	0.9	**1.08**	1.188	1.296
LCC (USD)	519,772	520,300	**522,945**	524,531	526,118

10. Conclusions

In this study, the available RE resources in the study area such as biomass and solar were considered to provide electricity and freshwater availability to five un-electrified villages in the Rayagada district of Odisha state in India. Due to the uncertainties in these RE resources, the power supply is not continuous. Hence, a feasibility study using three

different types of battery technologies such as lithium-ion (Li-Ion), nickel-iron (Ni-Fe), and lead-acid (LA) was considered in order to provide a continuous power supply in conjunction with a diesel generator (DG).

In order to find out an optimal configuration to electrify the study area, six different configurations were modelled using available RE resources and battery technologies. Initially, these six configurations were evaluated with load following (LF) and cycle charging (CC) strategies using the low-efficiency appliance usage-based scenario in the MATLAB© environment at an LPSP value of 0% with nine metaheuristic algorithms such as particle swarm optimization, grey wolf optimization, genetic algorithm, ant lion optimization, differential evolutionary algorithm, moth flame optimization, dragonfly algorithm, grasshopper optimization algorithm, and Salp Swarm Algorithm. According to the results, the Salp Swarm Algorithm showed its convergence and robustness efficiencies in comparison to other algorithms in order to find the global best optimal values. From the results of the low-efficiency appliance usage-based scenario, the Ni-Fe battery-based IHRES with LF strategy was found to be an optimal configuration. This was further evaluated with medium and high-efficiency appliance usage-based scenarios. The summary of these results are listed as follows:

The Ni-Fe battery-based IHRES with LF strategy using the low-efficiency appliance usage-based scenario, i.e., without DSM, obtained an LCC of USD 916,728, which is about 39% and 62% lower than the LCCs of LA (at 80% DOD) and Li-Ion (at 50% DOD) battery-based IHRES's LF strategies, respectively.

The Ni-Fe battery-based IHRES with LF strategy using the medium-efficiency appliance usage-based scenario, i.e., with DSM obtained an LCC of USD 613,841, which is about 33% lower than its LCC using low-efficiency appliance usage-based scenario.

The Ni-Fe battery-based IHRES with LF strategy using the high-efficiency appliance usage-based scenario, i.e., with DSM, obtained an LCC of USD 522,945, which is about 43% and 15% lower than its low and medium-efficiency appliance usage-based scenarios, respectively.

Finally, the sensitivity analysis was performed by varying the interest rate, biomass foliage collection rate, and diesel prices as compared to the other parameters, and the effect of the interest rate was found to have a major impact on the system performance.

The current study focused on demand-side management based on energy conservation. Using this study, power consumption in rural households as well as power production components in the study area can be reduced significantly. As a result, energy bills and total investment costs in the study area can be reduced. In future studies, with proper planning, peak load demands can be reduced by shifting non-peak load demand periods using energy conservation-based management. This methodology can significantly reduce the investment cost for the specific study area.

Author Contributions: Conceptualization, P.P.K. and R.S.S.N.; methodology, P.P.K. and V.S.; software, P.P.K. and S.A.S.; validation, M.A.H. and M.J.; formal analysis, P.P.K.; investigation, P.P.K. and M.J.; resources, P.P.K. and R.S.S.N.; data curation, V.S. and M.J.; writing—original draft preparation, P.P.K.; writing—review and editing, M.A.H. and S.A.S.; visualization, P.P.K. and R.S.S.N.; supervision, R.G. and Z.L.; project administration, M.J. and R.G.; funding acquisition, R.G. and Z.L. All authors have read and agreed to the published version of the manuscript.

Funding: This research was funded by SGS Grant from VSB—Technical University of Ostrava under grant number SP2022/21.

Institutional Review Board Statement: Not applicable.

Informed Consent Statement: Not applicable.

Data Availability Statement: Data available on request on correspondence to first author.

Conflicts of Interest: The authors declare no conflict of interest.

References

1. Maleki, A. Design and Optimization of Autonomous Solar-Wind-Reverse Osmosis Desalination Systems Coupling Battery and Hydrogen Energy Storage by an Improved Bee Algorithm. *Desalination* **2018**, *435*, 221–234. [CrossRef]
2. Iranmehr, H.; Aazami, R.; Tavoosi, J.; Shirkhani, M.; Azizi, A.-R.; Mohammadzadeh, A.; Mosavi, A.H.; Guo, W. Modeling the Price of Emergency Power Transmission Lines in the Reserve Market Due to the Influence of Renewable Energies. *Front. Energy Res.* **2022**, *9*, 792418. [CrossRef]
3. Sinha, S.; Chandel, S.S. Review of Software Tools for Hybrid Renewable Energy Systems. *Renew. Sustain. Energy Rev.* **2014**, *32*, 192–205. [CrossRef]
4. Bukar, A.L.; Tan, C.W. A Review on Stand-Alone Photovoltaic-Wind Energy System with Fuel Cell: System Optimization and Energy Management Strategy. *J. Clean. Prod.* **2019**, *221*, 73–88. [CrossRef]
5. Saremi, S.; Mirjalili, S.; Lewis, A. Advances in Engineering Software Grasshopper Optimisation Algorithm: Theory and Application. *Adv. Eng. Softw.* **2017**, *105*, 30–47. [CrossRef]
6. Mirjalili, S.; Mohammad, S.; Lewis, A. Advances in Engineering Software Grey Wolf Optimizer. *Adv. Eng. Softw.* **2014**, *69*, 46–61. [CrossRef]
7. Kennedy, J.; Eberhart, R. Particle Swarm Optimization. In Proceedings of the ICNN'95—International Conference on Neural Networks, Perth, WA, Australia, 27 November–1 December 1995; pp. 1942–1948.
8. Man, K.F.; Tang, K.S.; Kwong, S. Genetic Algorithms: Concepts and Applications. *IEEE Trans. Ind. Electron.* **1996**, *43*, 519–534. [CrossRef]
9. Bukar, A.L. Optimal Sizing of an Autonomous Photovoltaic/Wind/Battery/Diesel Generator Microgrid Using Grasshopper Optimization Algorithm. *Sol. Energy* **2019**, *188*, 685–696. [CrossRef]
10. Mirjalili, S.; Gandomi, A.H.; Zahra, S.; Saremi, S. Salp Swarm Algorithm: A Bio-Inspired Optimizer for Engineering Design Problems. *Adv. Eng. Softw.* **2017**, *114*, 163–191. [CrossRef]
11. Liang, M.; Fu, C.; Xiao, B.; Luo, L.; Wang, Z. A Fractal Study for the Effective Electrolyte Diffusion through Charged Porous Media. *Int. J. Heat Mass Transf.* **2019**, *137*, 365–371. [CrossRef]
12. Liang, M.; Liu, Y.; Xiao, B.; Yang, S.; Wang, Z.; Han, H. An Analytical Model for the Transverse Permeability of Gas Diffusion Layer with Electrical Double Layer Effects in Proton Exchange Membrane Fuel Cells. *Int. J. Hydrogen Energy* **2018**, *43*, 17880–17888. [CrossRef]
13. Ramesh, M.; Saini, R.P. Dispatch Strategies Based Performance Analysis of a Hybrid Renewable Energy System for a Remote Rural Area in India. *J. Clean. Prod.* **2020**, *259*, 120697. [CrossRef]
14. Patel, A.M.; Singal, S.K. Optimal Component Selection of Integrated Renewable Energy System for Power Generation in Stand-Alone Applications. *Energy* **2019**, *175*, 481–504. [CrossRef]
15. Rajanna, S.; Saini, R.P. Modeling of Integrated Renewable Energy System for Electri Fi Cation of a Remote Area in India. *Renew. Energy* **2020**, *90*, 175–187. [CrossRef]
16. Bhatt, A.; Sharma, M.P.; Saini, R.P. Feasibility and Sensitivity Analysis of an Off-Grid Micro Hydro–Photovoltaic–Biomass and Biogas–Diesel–Battery Hybrid Energy System for a Remote Area in Uttarakhand State, India. *Renew. Sustain. Energy Rev.* **2016**, *61*, 53–69. [CrossRef]
17. Upadhyay, S.; Sharma, M.P. Selection of a Suitable Energy Management Strategy for a Hybrid Energy System in a Remote Rural Area of India. *Energy* **2016**, *94*, 352–366. [CrossRef]
18. Li, C.; Zhou, D.; Wang, H.; Lu, Y.; Li, D. Techno-Economic Performance Study of Stand-Alone Wind/Diesel/Battery Hybrid System with Different Battery Technologies in the Cold Region of China. *Energy* **2020**, *192*, 116702. [CrossRef]
19. Durlinger, B.; Reinders, A.; Toxopeus, M. A Comparative Life Cycle Analysis of Low Power PV Lighting Products for Rural Areas in South East Asia. *Renew. Energy* **2012**, *41*, 96–104. [CrossRef]
20. Shezan, S.K.A.; Julai, S.; Kibria, M.A.; Ullah, K.R.; Saidur, R.; Chong, W.T.; Akikur, R.K. Performance Analysis of an Off-Grid Wind-PV (Photovoltaic) -Diesel- Battery Hybrid Energy System Feasible for Remote Areas. *J. Clean. Prod.* **2016**, *125*, 121–132. [CrossRef]
21. Rodríguez-Gallegos, C.D.; Gandhi, O.; Bieri, M.; Reindl, T.; Panda, S.K. A Diesel Replacement Strategy for Off-Grid Systems Based on Progressive Introduction of PV and Batteries: An Indonesian Case Study. *Appl. Energy* **2018**, *229*, 1218–1232. [CrossRef]
22. Pina, A.; Ferrão, P.; Fournier, J.; Lacarrière, B.; Corre, O. Le ScienceDirect ScienceDirect ScienceDirect Techno-Economic Analysis of Hybrid System Assessing the Feasibility of Using the Heat Demand-Outdoor Temperature Function for a District Heat Demand Forecast for Rural Electrification in Cambodia. *Energy Procedia* **2017**, *138*, 524–529. [CrossRef]
23. Kohsri, S.; Meechai, A.; Prapainainar, C. Chemical Engineering Research and Design Design and Preliminary Operation of a Hybrid Syngas/Solar PV/Battery Power System for off-Grid Applications: A Case Study in Thailand. *Chem. Eng. Res. Des.* **2018**, *131*, 346–361. [CrossRef]
24. Kim, H.; Yong, T. Independent Solar Photovoltaic with Energy Storage Systems (ESS) for Rural Electri Fi Cation in Myanmar. *Renew. Sustain. Energy Rev.* **2018**, *82*, 1187–1194. [CrossRef]
25. Lozano, L.; Querikiol, E.M.; Abundo, M.L.S.; Bellotindos, L.M. Techno-Economic Analysis of a Cost-Effective Power Generation System for off-Grid Island Communities: A Case Study of Gilutongan Island, Cordova, Cebu, Philippines. *Renew. Energy* **2019**, *140*, 905–911. [CrossRef]

26. Paul, S.; Schirmer, T.; Kairies, K.; Axelsen, H.; Uwe, D. Comparison of o Ff -Grid Power Supply Systems Using Lead-Acid and Lithium- Ion Batteries. *Sol. Energy* **2018**, *162*, 140–152. [CrossRef]
27. Kaabeche, A.; Bakelli, Y. Renewable Hybrid System Size Optimization Considering Various Electrochemical Energy Storage Technologies. *Energy Convers. Manag.* **2019**, *193*, 162–175. [CrossRef]
28. Bhattacharyya, S.C. *Energy Economics*; Springer: London, UK, 2011; ISBN 9780857292674.
29. Rajanna, S.; Saini, R.P. Employing Demand Side Management for Selection of Suitable Scenario-Wise Isolated Integrated Renewal Energy Models in an Indian Remote Rural Area. *Renew. Energy* **2016**, *99*, 1161–1180. [CrossRef]
30. Chauhan, A.; Saini, R.P. Techno-Economic Optimization Based Approach for Energy Management of a Stand-Alone Integrated Renewable Energy System for Remote Areas of India. *Energy* **2016**, *94*, 138–156. [CrossRef]
31. Zheng, Y.; Jenkins, B.M.; Kornbluth, K.; Kendall, A.; Træholt, C. Optimization of a Biomass-Integrated Renewable Energy Microgrid with Demand Side Management under Uncertainty. *Appl. Energy* **2018**, *230*, 836–844. [CrossRef]
32. Wang, X.; Palazoglu, A.; El-farra, N.H. Operational Optimization and Demand Response of Hybrid Renewable Energy Systems. *Appl. Energy* **2015**, *143*, 324–335. [CrossRef]
33. Marzband, M.; Ghadimi, M.; Sumper, A.; Domínguez-garcía, J.L. Experimental Validation of a Real-Time Energy Management System Using Multi-Period Gravitational Search Algorithm for Microgrids in Islanded Mode. *Appl. Energy* **2014**, *128*, 164–174. [CrossRef]
34. Matallanas, E.; Castillo-cagigal, M.; Gutiérrez, A.; Monasterio-huelin, F.; Caamaño-martín, E. Neural Network Controller for Active Demand-Side Management with PV Energy in the Residential Sector. *Appl. Energy* **2012**, *91*, 90–97. [CrossRef]
35. Gudi, N.; Wang, L.; Devabhaktuni, V. Electrical Power and Energy Systems A Demand Side Management Based Simulation Platform Incorporating Heuristic Optimization for Management of Household Appliances. *Int. J. Electr. Power Energy Syst.* **2012**, *43*, 185–193. [CrossRef]
36. Kyriakarakos, G.; Piromalis, D.D.; Dounis, A.I.; Arvanitis, K.G.; Papadakis, G. Intelligent Demand Side Energy Management System for Autonomous Polygeneration Microgrids. *Appl. Energy* **2013**, *103*, 39–51. [CrossRef]
37. Kallel, R.; Boukettaya, G.; Krichen, L. Demand Side Management of Household Appliances in Stand-Alone Hybrid Photovoltaic System. *Renew. Energy* **2015**, *81*, 123–135. [CrossRef]
38. Venkatappiah, B. Rural Electrification Corporation Limited. *Econ. Political Wkly.* **1971**, *6*, 2073–2076.
39. Storn, R. Differential Evolution—A Simple and Efficient Heuristic for Global Optimization over Continuous Spaces. *J. Glob. Optim.* **1997**, *11*, 341–359. [CrossRef]
40. Mirjalili, S. Advances in Engineering Software the Ant Lion Optimizer. *Adv. Eng. Softw.* **2015**, *83*, 80–98. [CrossRef]
41. Mirjalili, S. Moth-Flame Optimization Algorithm: A Novel Nature-Inspired Heuristic Paradigm. *Knowl.-Based Syst.* **2015**, *89*, 228–249. [CrossRef]
42. Mirjalili, S. Dragonfly Algorithm: A New Meta-Heuristic Optimization Technique for Solving Single-Objective, Discrete, and Multi-Objective Problems. *Neural Comput. Appl.* **2016**, *27*, 1053–1073. [CrossRef]
43. Kumar, P.P.; Saini, R.P. Optimization of an Off-Grid Integrated Hybrid Renewable Energy System with Different Battery Technologies for Rural Electrification in India. *J. Energy Storage* **2020**, *32*, 101912. [CrossRef]
44. Enersol Biopower. Available online: http://enersolbiopower.com/ (accessed on 5 May 2020).
45. Chauhan, A.; Saini, R.P. Discrete Harmony Search Based Size Optimization of Integrated Renewable Energy System for Remote Rural Areas of Uttarakhand State in India. *Renew. Energy* **2016**, *94*, 587–604. [CrossRef]
46. Kumar, P.P.; Saini, R.P. Optimization of an Off-Grid Integrated Hybrid Renewable Energy System with Various Energy Storage Technologies Using Different Dispatch Strategies. *Energy Sources Part A Recover. Util. Environ. Eff.* **2020**, *32*, 101912. [CrossRef]
47. Ogunjuyigbe, A.S.O.; Ayodele, T.R.; Akinola, O.A. Optimal Allocation and Sizing of PV/Wind/Split-Diesel/Battery Hybrid Energy System for Minimizing Life Cycle Cost, Carbon Emission and Dump Energy of Remote Residential Building. *Appl. Energy* **2016**, *171*, 153–171. [CrossRef]
48. Tu, T.; Rajarathnam, G.P.; Vassallo, A.M. Optimization of a Stand-Alone Photovoltaic e Wind e Diesel e Battery System with Multi-Layered Demand Scheduling. *Renew. Energy* **2019**, *131*, 333–347. [CrossRef]
49. Upadhyay, S.; Sharma, M.P. Development of Hybrid Energy System with Cycle Charging Strategy Using Particle Swarm Optimization for a Remote Area in India. *Renew. Energy* **2015**, *77*, 586–598. [CrossRef]
50. Iron Edison. Available online: https://ironedison.com/store (accessed on 10 January 2020).
51. Trojan Battery Company. Available online: https://www.trojanbattery.com/ (accessed on 12 January 2020).
52. Victron Energy Blue Power. Available online: https://www.victronenergy.com/batteries (accessed on 15 January 2020).
53. Reserve Bank of India. Available online: https://www.rbi.org.in/home.aspx (accessed on 12 February 2020).
54. Vikram Solar. Available online: https://www.vikramsolar.com/ (accessed on 25 May 2020).
55. Mechanical Structure Cost of PV Panel. Available online: https://www.loomsolar.com/products/loom-solar-2-row-design-6-panel-stand-375-watt?gclid=CjwKCAjwsan5BRAOEiwALzomXxjAoKPGLLYkGRoWRgkR7mAros-FbPGeWeNhzvOqId-TRQESPrWq3xoC3CAQAvD_BwE (accessed on 12 May 2020).
56. Cummins Diesel Generators. Available online: https://www.cummins.com/en/in/company/cummins-india (accessed on 11 August 2020).
57. Kirloskar Diesel Generators. Available online: https://www.koeligreen.in/index.php#genset (accessed on 15 August 2020).